Thermal and structural modeling of the Scillato wedge-top basin source-to-sink system: Insights into Sicilian fold-and-thrust belt building (Italy)

Martina Balestra[1,†], Sveva Corrado[1], Luca Aldega[2], Maurizio Gasparo Morticelli[3], Attilio Sulli[3], Jean-Luc Rudkiewicz[4], and William Sassi[4]
[1]*Dipartimento di Scienze, Università Roma Tre, 00146 Rome, Italy*
[2]*Dipartimento di Scienze della Terra, Sapienza Università di Roma, 00185 Rome, Italy*
[3]*Dipartimento di Scienze della Terra e del Mare, Università di Palermo, 90123 Palermo, Italy*
[4]*IFP Energies Nouvelles, 92852 Rueil-Malmaison, France*

ABSTRACT

Temperature-dependent clay mineral assemblages, vitrinite reflectance, and one-dimensional (1-D) thermal and three-dimensional (3-D) geological modeling of a Neogene wedge-top basin in the Sicilian fold-and-thrust belt and its pre-orogenic substratum allowed us to: (1) define the burial history of the sedimentary succession filling the wedge-top basin and its substratum, (2) reconstruct the wedge-top basin geometry, depocenter migration, and sediment provenance through time in the framework of a source-to-sink system, and (3) shed new light into the kinematic evolution of the Apennine-Maghrebian fold-and-thrust belt.

The pre-orogenic substratum of the Scillato basin shows an increase in levels of thermal maturity as a function of stratigraphic age that is consistent with maximum burial to 3.5 km in deep diagenetic conditions. In detail, R_o% values range from 0.40% to 0.94%, and random ordered illite-smectite (I-S) first converts to short-range ordered structures and then evolves to long-range ordered structures at the base of the Imerese unit. The wedge-top basin fill experienced shallow burial (~2 km) and levels of thermal maturity in the immature stage of hydrocarbon generation and early diagenesis. Vitrinite reflectance and mixed-layer I-S values show two populations of authigenic and inherited phases. The indigenous population corresponds to macerals with R_o% values of 0.33%–0.45% and I-S with no preferred sequence in stacking of layers, whereas the reworked group corresponds to macerals with R_o% values of 0.42%–0.47% and short-range ordered I-S with no correlation as a function of depth.

Authigenic and reworked components of the Scillato basin fill allowed us to unravel sediment provenance during the Neogene, identifying two main source areas feeding the wedge-top basin (crystalline units of the European domain and sedimentary units of the African domain), and to detect an early phase of exhumation driven by low-angle extensional faults that predated Neogene compression.

INTRODUCTION

Source-to-sink systems consist of areas that contribute to erosion (e.g., hillslopes), transportation (e.g., rivers), and deposition (e.g., river floodplains, deltas, deep marine basins) of sediments within a denudation-accumulation system (Allen, 2008; Sømme et al., 2009; Allen and Allen, 2013; Michael et al., 2014). Fold-and-thrust belts and their foreland basin systems (DeCelles and Giles, 1996) represent source-to-sink systems closely linked in space and through time (Barnes and Heins, 2008). Their burial evolution, uplift, and exhumation are recorded by the sedimentary successions and architecture of associated basins. In particular, wedge-top basins, lying on top of orogenic belts, are affected by paleotopographic and structural variations related to synorogenic deformation (Butler and Grasso, 1993; Pinter et al., 2016). Thus, the study of wedge-top basins provides essential pieces of information on vertical movements and tectonic evolution of the source areas for sediments (e.g., orogenic belt).

However, the amounts and timing of vertical motion in frontal parts of fold-and-thrust belts are not easily quantifiable because burial is generally limited to a few kilometers, and very few techniques may be applied to sedimentary rocks to detect tectonic thickening and exhumation (e.g., fission track and U-Th/He on apatite, organic matter optical analysis, X-ray diffraction of clay minerals; Garver et al., 1999; Jolivet et al., 2007; Corrado et al., 1998, 2009, 2010; Zattin et al., 2011; Whitchurch et al., 2011; Izquierdo-Llavall et al., 2013; Di Paolo et al., 2014; Caricchi et al., 2015; Aldega et al., 2017, 2018; Schito et al., 2018).

Recently, the timing and modes of deformation of the Sicilian fold-and-thrust belt in the study area were unraveled by combining sedimentological and stratigraphic data from the wedge-top basins succession with structural analysis of its deformed substratum (Gugliotta, 2012; Gugliotta and Gasparo Morticelli, 2012; Gugliotta et al., 2013, 2014). Nevertheless, this approach provided only hints on the kinematic evolution of the Sicilian fold-and-thrust belt without quantifying and validating tectonic thickening, sedimentary loads, and amounts of exhumation.

Thus, we combined paleothermal indicators (e.g., vitrinite reflectance and illite content in mixed-layer illite-smectite [I-S]) and organic petrographic studies of the fine fraction of sediments from the Scillato wedge-top basin and its deformed substratum with one-dimensional (1-D) thermal and three-dimensional (3-D) geometrical modeling to: (1) define the burial and thermal history of the sedimentary succession filling the Scillato wedge-top basin and its substratum, (2) reconstruct the wedge-top basin geometry, depocenter migration, and sediment provenance through time, and (3) shed new light into the kinematic evolution of the Apennine-Maghrebian fold-and-thrust belt, suggesting an early phase of exhumation driven by low-angle extensional faults, which predated Neogene compression.

[†] martina.balestra@uniroma3.it

GSA Bulletin; https://doi.org/10.1130/B35078.1; 10 figures; 1 table.

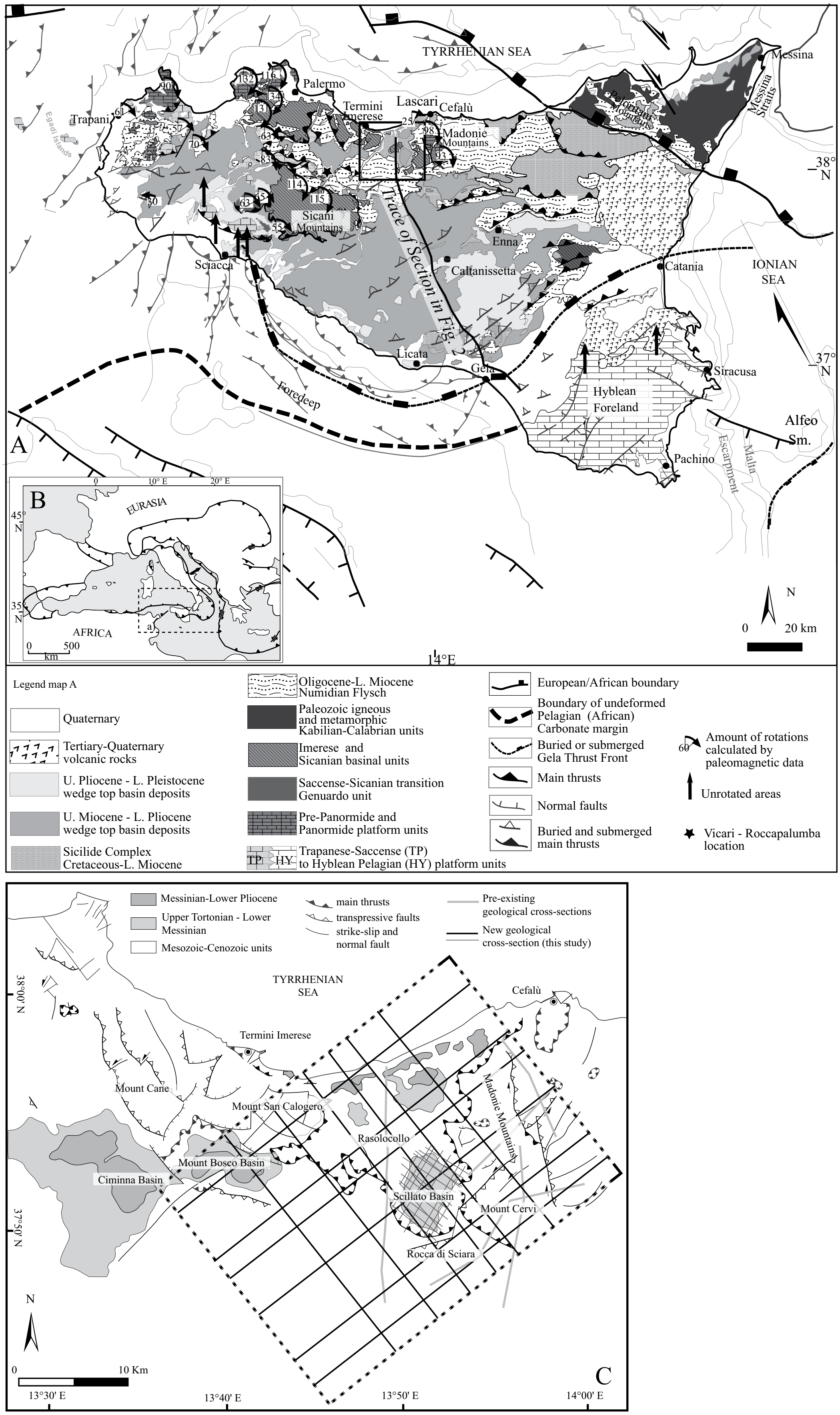
TYRRHENIAN SEA
Messina
Peloritani Mountains
Messina Straits
Palermo
Termini Imerese
Lascari
Cefalù
Madonie Mountains
Trapani
Egadi Islands
Sicani Mountains
Sciacca
Trace of Section in Fig. 2
Enna
Caltanissetta
Catania
IONIAN SEA
Licata
Gela
Siracusa
Hyblean Foreland
Foredeep
Alfeo Sm.
Malta Escarpment
Pachino
38° N
37° N
A
90
61
57
70
50
132
116
34
131
63
83
114
115
63
55
23
98
93
B
0
10° E
20° E
45° N
35° N
EURASIA
AFRICA
0 500 km
a
N
0 20 km
14°E
Legend map A
Quaternary
Tertiary-Quaternary volcanic rocks
U. Pliocene - L. Pleistocene wedge top basin deposits
U. Miocene - L. Pliocene wedge top basin deposits
Sicilide Complex Cretaceous-L. Miocene
Oligocene-L. Miocene Numidian Flysch
Paleozoic igneous and metamorphic Kabilian-Calabrian units
Imerese and Sicanian basinal units
Saccense-Sicanian transition Genuardo unit
Pre-Panormide and Panormide platform units
TP HY
Trapanese-Saccense (TP) to Hyblean Pelagian (HY) platform units
European/African boundary
Boundary of undeformed Pelagian (African) Carbonate margin
Buried or submerged Gela Thrust Front
Main thrusts
Normal faults
Buried and submerged main thrusts
60
Amount of rotations calculated by paleomagnetic data
Unrotated areas
Vicari - Roccapalumba location
Messinian-Lower Pliocene
Upper Tortonian - Lower Messinian
Mesozoic-Cenozoic units
main thrusts
transpressive faults
strike-slip and normal fault
Pre-existing geological cross-sections
New geological cross-section (this study)
TYRRHENIAN SEA
Cefalù
Termini Imerese
Mount Cane
Mount San Calogero
Rasolocollo
Madonie Mountains
Mount Bosco Basin
Ciminna Basin
Scillato Basin
Mount Cervi
Rocca di Sciara
38°00' N
37°50' N
N
0 10 Km
C
13°30' E
13°40' E
13°50' E
14°00' E

Figure 1. (A)

←

Figure 1. (A) Geological map of Sicily (modified and redrawn after Gasparo Morticelli et al., 2015). The black rectangle indicates the study area. Palaeomagnetic data are from Channell et al. (1990), Grasso et al. (1987), and Speranza et al. (2003). (B) Tectonic map of central Mediterranean area (modified and redrawn after Gasparo Morticelli et al., 2015). (C) Simplified structural map of the central-northern Sicily showing major Miocene–Pliocene basins and large-scale tectonic structures (modified after Gugliotta and Gasparo Morticelli, 2012). Dashed rectangle indicates the areal extent of the three-dimensional geological model. Traces of preexisting (gray lines) and new geological section (thick and thin black lines) built using Move software are also indicated. Preexisting cross sections are from Catalano et al. (2011). U.—Upper; L.—Lower.

In the end, we propose that the integration of the aforementioned approach with reconstruction of vertical motions of wedge-top basin margins can be a useful tool for unraveling source-to-sink systems in fold-and-thrust belts.

GEOLOGICAL SETTING

Sicily is located in the central Mediterranean area as a segment of the Apennine-Maghrebian chain (Fig. 1), which originated from the tectonic inversion of the African continental passive margin (Catalano and D'Argenio, 1982; Roure et al., 1990; Catalano et al., 1996; S. Catalano et al., 2008). The Sicilian fold-and-thrust belt has been developing since the early Miocene as a SSE-verging chain resulting from the postcollisional convergence between Africa and Europe (Dercourt et al., 1986; Dewey et al., 1989; Catalano et al., 1996, 2000; Faccenna et al., 2004) and the rollback of the subduction hinge of Ionian lithosphere (Caputo et al., 1970; Doglioni et al., 1999; Faccenna et al., 2001). These processes are responsible for deformation and tectonic transport of different paleogeographic domains, now stacked to form the tectonic wedge (Fig. 2; Finetti et al., 2005; Catalano et al., 2013; Di Paolo et al., 2012, 2014; Gasparo Morticelli et al., 2015). From the innermost to the outermost domain, they are: (1) the European domain, exposed in the NE part of Sicily (e.g., Peloritani Mountains), which is mainly constituted by crystalline and metamorphic units (Vignaroli et al., 2008; Aldega et al., 2011); (2) the Tethyan domain (Sicilide Complex), which corresponds to Cretaceous–Lower Miocene pelagic successions detached from their substratum (Ogniben, 1960; Bianchi et al., 1989; Catalano et al., 1996; Corrado et al., 2009); and (3) the African domain, composed of different tectono-stratigraphic units subdivided into deep-water (Imerese and Sicano units), shallow-water (Panormide unit), and carbonate-pelagic platforms (Trapanese and Saccense units; Catalano and D'Argenio, 1982; Catalano et al., 2000; Nigro and Renda, 1999; Zarcone et al., 2010).

A foreland basin developed from the latest Oligocene to early Miocene, which was subsequently filled by the Numidian Flysch (Catalano et al., 1989; Nigro and Renda, 2000; Grasso, 2001). The foreland basin system progressively migrated toward the Hyblean foreland, which is exposed in southeastern Sicily and extends offshore along the Sicily Channel in the Mediterranean Sea (Catalano et al., 1989; Butler and Grasso, 1993; Nigro and Renda, 2000; Grasso, 2001; Gasparo Morticelli et al., 2015).

Since the middle Miocene, the study area has recorded a polyphase deformation. During the Serravallian, the emplacement of allochthonous units (Numidian Flysch, Sicilide Complex, Imerese-Sicano units) onto the Trapanese-Hyblean foreland through low-angle regional thrusts produced shallow-seated structures (Event I in Fig. 3) with a present-day southwestward tectonic transport direction (Catalano et al., 2000; Avellone et al., 2010; Gasparo Morticelli et al., 2015). During the latest Tortonian–early Pleistocene, ongoing compressional deformation gave rise to the nucleation of deep-seated thrusts, which refolded and breached the previously stacked thin-skinned tectonic units along high-angle transpressive faults (Event II in Fig. 3; Bello et al., 2000; Catalano et al., 2000; Gasparo Morticelli et al., 2015).

Structures generated as a consequence of these two tectonic events are strongly noncoaxial, and their present-day setting can be explained by the occurrence of large vertical-axis clockwise rotations (Fig. 1; Channell et al., 1980, 1990; Grasso et al., 1987; Oldow et al., 1990; Speranza et al., 1999, 2003, 2018; Avellone and Barchi, 2003; Guarnieri, 2004; Monaco and De Guidi, 2006; Avellone et al., 2010; Cifelli and Mattei, 2010; Barreca and Monaco, 2013), which decrease from the internal units (e.g., Imerese and Panormide units ~130°) toward the foreland (e.g., no rotation in the Sciacca area). Part of this rotation (~25°) is post–early Pliocene in age (Grasso et al., 1987). Wedge-top basins, including the Scillato Basin, record these two tectonic events with their shape, internal architecture, and sedimentary fill (Gugliotta et al., 2014).

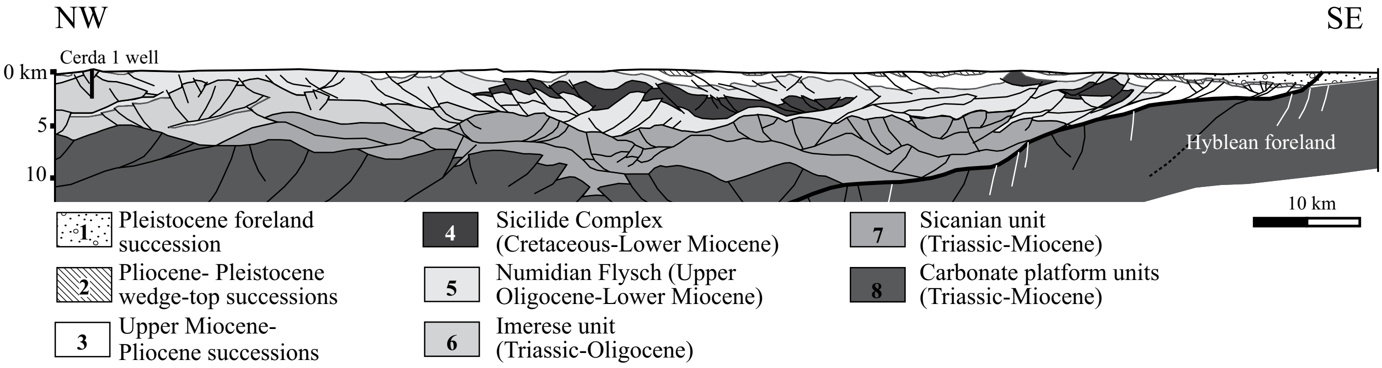

Figure 2. Regional cross section (for location, see Fig. 1) showing the overall architecture of the Sicilian wedge (modified and redrawn after Catalano et al., 2013). Interpretation at depth is from the seismic reflection profile of the SI.RI.PRO (Sismica a Riflessione Profonda) project. Black lines indicate reverse faults; thick black line indicates the sole thrust; white lines indicate normal faults.

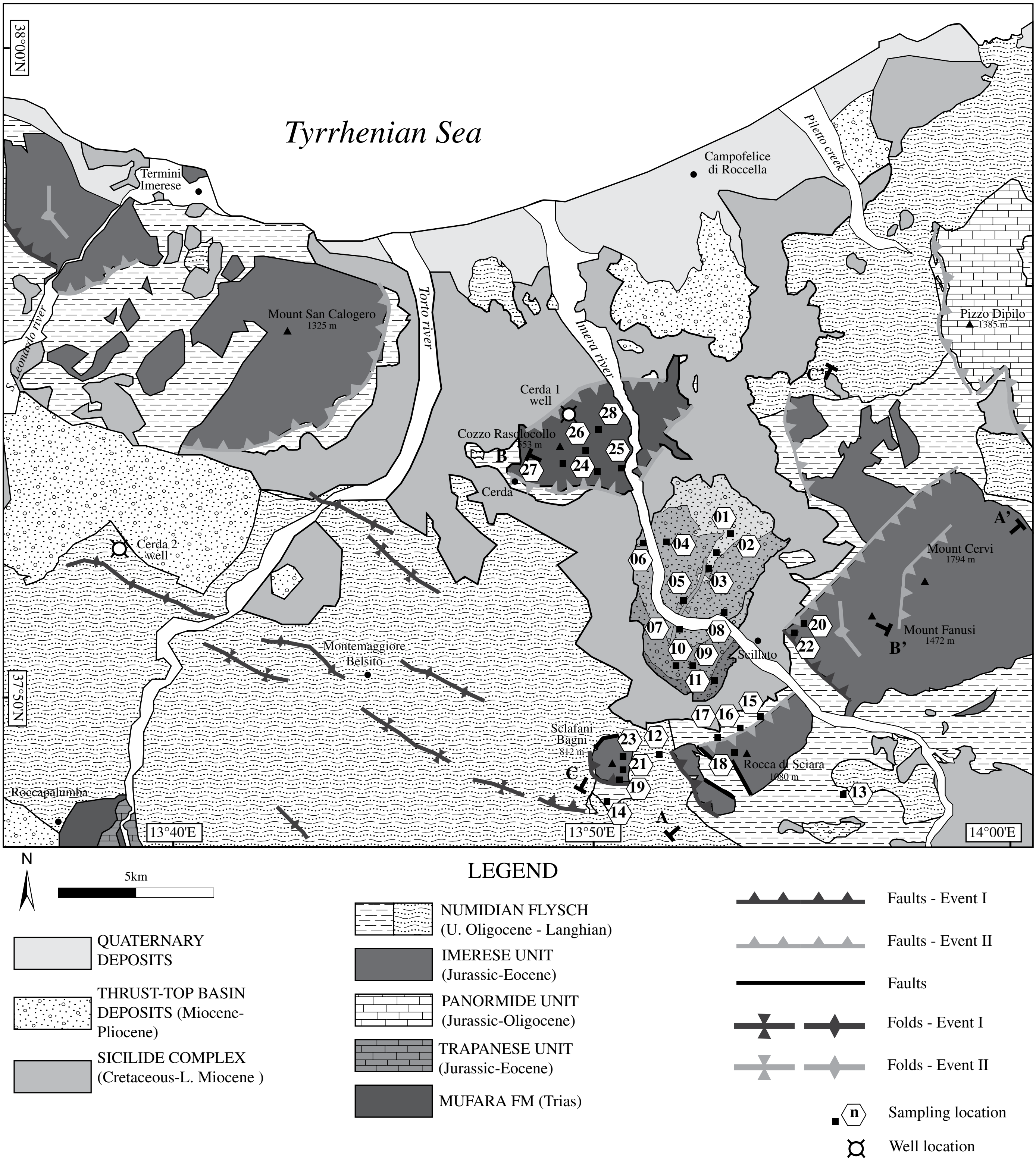

Figure 3. Tectonic sketch map of the study area with sampling sites (modified after Catalano et al., 2011). Locations of cross sections in Figures 7 and 8 are shown. U—Upper; L—Lower.

Deformed Pre-Orogenic Substratum of the Scillato Wedge-Top Basin

The substratum of the Scillato wedge-top basin is made up of thrust sheets mainly deforming the Imerese unit (Upper Triassic–Eocene), the Numidian Flysch (Upper Oligocene–Lower Miocene), the Sicilide Complex (Cretaceous–Lower Miocene), and the Lercara unit (Permian–Triassic) exposed in the northwestern part of the study area (Fig. 3; Mount Rasolocollo-Cerda area; Di Stefano and Gullo, 1997; Giunta et al., 2000).

The Imerese marly-cherty-calcareous succession in pelagic basin facies is exposed along the Mount Cervi–Rocca di Sciara–Sclafani Bagni and the Mount San Calogero structures (Fig. 3). From the bottom, the Imerese succession (Fig. 4) is subdivided into: the Carnian Mufara Formation (~300 m thick); the Carnian–Rethian cherty limestones (Scillato Formation, ~650 m thick); the Lower Jurassic dolostones of the Fanusi Formation up to 200 m thick; the Lower Jurassic–Upper Cretaceous shales, limestones, and radiolarites of the Crisanti Formation, with a thickness of 350 m, and the Eocene–Lowermost Oligocene marls and limestones of the Caltavuturo Formation, which are ~150 m thick. Upper Oligocene–Langhian Numidian Flysch (from 300 m up to 2,000 m thick) covers the Caltavuturo Formation, and it is mainly composed of claystones/siltstones with subordinate quartzarenites evolving to quartzarenites alternating with thin-bedded claystones and siltstones toward the top.

The Sicilide Complex is made up of Cretaceous–Lower Miocene highly deformed claystones, marls, and limestones up to 300 m thick. The Imerese and Sicilide successions (Fig. 4) also show strong vertical and lateral variations in mechanical proprieties (Avellone et al., 2010), which affect the geometry of the Sicilian fold-and-thrust belt, generating detachment levels and disharmonic and/or polyharmonic folds. Major detachment levels occur in the Mufara Formation, in the basal portion of the Numidian Flysch, and in the Sicilide Complex.

The Lercara unit has been drilled in several wells in the Sicilian fold-and-thrust belt (e.g., Cerda 1, Cerda 2, Vicari 1, Roccapalumba 1; Miuccio et al., 2000; Basilone et al., 2016) and consists of a Permian–Triassic siliciclastic and carbonate succession. Various authors (Catalano et al., 1991; Flügel et al., 1991; Kozur et al., 1996; Di Stefano and Gullo, 1997; Di Stefano et al., 2012; Basilone et al., 2016) have described the Lercara unit as made up of turbidites passing upward into deep-water limestones and siliciclastic deposits with a minimum thickness of ~2.1 km.

The subsurface extent of the Triassic deposits in the Cerda 1 well (for location, see Figs. 2 and 3) is ~3 km (probably due to tectonic thickening, since the maximum thickness evaluated for the Mufara Formation is ~300 m; Basilone et al., 2016), where they are mainly composed of claystones locally rich in organic matter, limestones, calcareous breccias, and quartz-rich sandstones. The Lercara unit in western Sicily shows the juxtaposition of the Numidian Flysch onto the Mufara Formation (Fig. 3). This boundary has been interpreted either as an extensional detachment (Giunta et al., 2000) or a younger-on-older thrust (Di Stefano and Gullo, 1997). In the study area, the boundary between the Mufara Formation and the Numidian Flysch is not well exposed and understood, and the Mufara Formation is bordered to the east and west by NNE-SSW–trending high-angle faults (Fig. 3).

Scillato Wedge-Top Basin

The Scillato wedge-top basin is located in the central-northern sector of the Sicilian fold-and-thrust belt, along the western edge of the Madonie Mountains (Figs. 1 and 3). It consists of a local NNE-SSW–oriented structural trough ~3.5 km wide and ~6 km long. The basin is bounded by the Mount Cervi–Rocca di Sciara–Sclafani Bagni structural highs to the SE and the Mount San Calogero structure to the NW. The Upper Serravallian–Upper Tortonian basin fill is composed of ~1250-m-thick open-marine and delta-river siliciclastic sediments (Gugliotta and Gasparo Morticelli, 2012; Gugliotta et al., 2014). The sedimentary succession is subdivided into the Castellana Sicula and Terravecchia Formations (Fig. 4).

The Castellana Sicula Formation is constituted by 50-m-thick hemipelagic clays, siltstones, gravity-flow sandstones, and conglomerates of late Serravallian–early Tortonian age deposited in an outer-shelf to slope setting.

The Terravecchia Formation (Upper Tortonian) is up to 1200 m thick, and it is constituted by a coarsening-to-fining-upward and then fining-to-coarsening upward sedimentary succession made up of different lithotypes: (1) conglomerates and sandstones (alluvial and paralic facies), (2) sandstones, and (3) marls and clays (transitional to shallow-marine facies). In detail, it is subdivided into three members bounded by unconformities, namely, from bottom (Figs. 3 and 4): Terravecchia 1, Terravecchia 2–3, and Terravecchia 1b (TS1, TS2, and RS, respectively, *in* Gugliotta and Gasparo Morticelli, 2012). The Terravecchia 1 member, ~300 m thick, is mainly composed of red conglomerates with metamorphic pebbles and sandstones passing upward to claystones/siltstones indicating a gravelly braided fluvial system. The Terravecchia 2–3 member, up to 800 m thick, is mainly composed of interbedded siltstones, cross-bedded sandstones to siltites, and clayey siltites. The Terravecchia 1b, 100 m thick, is mainly composed of silts and clays interbedded with conglomeratic bodies passing to cross-bedded sandstones and conglomerates.

METHODS AND MATERIALS

Organic Matter Optical Analysis

Organic matter optical analysis was performed on dispersed organic matter from twenty-three samples. Eleven samples were collected from claystones/siltstones of the Castellana Sicula Formation and the sandy portions of the Terravecchia Formation. Twelve samples were collected from the deformed substratum of the Scillato wedge-top basin (Fig. 3), and they pertain to claystones/siltstones of the Mufara Formation located in the Mount Rasolocollo-Cerda area, to the Crisanti organic-rich shales, and to the Numidian Flysch sandstones/claystones exposed along the Mount Cervi–Rocca di Sciara–Sclafani Bagni structure. Samples were collected at distance >1 m from major faults in order to avoid potential temperature increase due to frictional heating (Balsamo et al., 2014). Whole-rock samples were crushed in an agate mortar, mounted in epoxy resin, and polished according to standard procedures (Bustin et al., 1990). Vitrinite reflectance (R_o%) measurements were performed on randomly oriented grains using a Zeiss Axioplan microscope, under oil immersion (n = 1.518) in reflected monochromatic nonpolarized light, equipped with a J&M reflectance system. Various reflectance standards (R_o% = 0.426%, 0.595%, and 0.905%) were used for calibration. The number of measurements ranged from 15 in samples with small amounts of organic matter to 50 for organic matter–rich specimens. On each sample, measurements were carried out on unaltered, nonoxidized, and unfractured fragments of humite-vitrinite macerals and coal seams. Mean reflectance values were calculated using the arithmetic mean of these measurements.

X-Ray Diffraction (XRD) Analysis

A suite of twenty-seven samples (Fig. 3) was collected from the wedge-top succession (11 samples) and its substratum (16 samples). In the Scillato wedge-top basin, samples were collected from claystones/siltstones of the Castellana Sicula and Terravecchia Formations. In the substratum, samples were from the Mufara Formation, the shales of the Crisanti Formation,

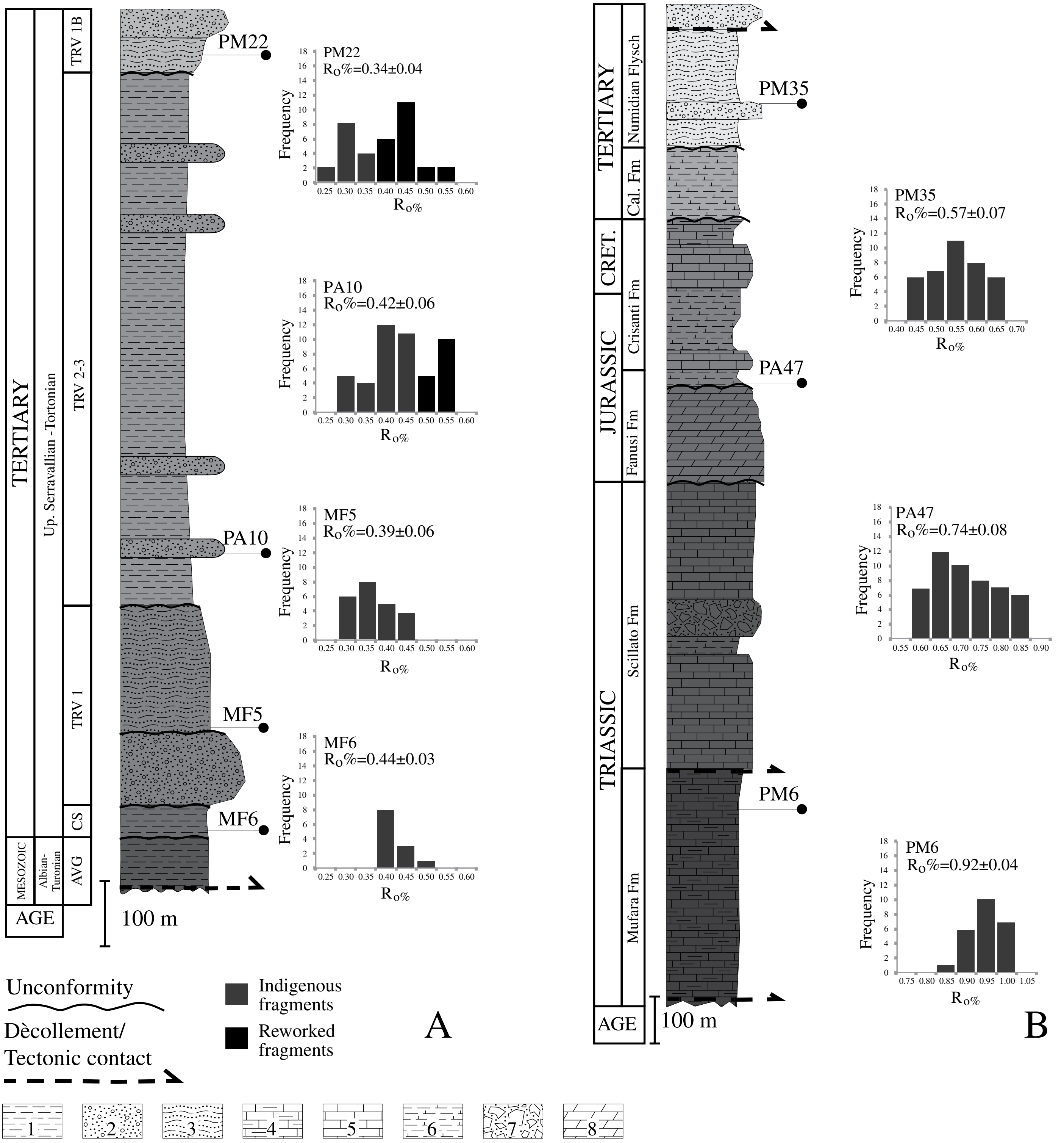

Figure 4. Simplified stratigraphic columns of (A) the Scillato wedge-top basin and (B) Imerese unit successions, with representative histograms of vitrinite reflectance data. Main unconformities and detachment levels are indicated. Cal—Caltavuturo Formation; AVG—Sicilide Complex; CS—Castellana Sicula Formation; TRV1—Terravecchia 1 member; TRV2–3, TRV1B—Terravecchia 2–3 and 1b members. 1—claystones/shales; 2—gravelly sandstones/conglomerates; 3—sandstones; 4—alternating limestones/shales/sandstones; 5—limestones; 6—marls; 7—breccias; 8—dolostones. Up.—Upper.

the reddish marls of the Caltavuturo Formation, and the Numidian Flysch cropping out along the Mount Cervi–Rocca di Sciara–Sclafani Bagni structure. Qualitative and semiquantitative analyses of the <2 μm grain-size fraction (equivalent spherical diameter) were performed using a Scintag X1 X-ray system (CuKα radiation). After centrifugation, the suspension containing the <2 μm grain-size fraction was decanted, pipetted, and dried at room temperature on glass slides to produce a thin, highly oriented aggregate. Oriented air-dried samples were scanned from 1° to 48° 2θ with a step size of 0.05° 2θ and a count time of 4 s per step at 40 kV and 45 mA. The presence of expandable clays was determined for samples treated with ethylene glycol at 25 °C for 24 h. Ethylene glycol–solvated samples were scanned at the same conditions as air-dried aggregates, with a scanning interval of 1°–30° 2θ. Expandability measurements were determined according to Moore and Reynolds (1997) by using the Δ2θ method after decomposing the composite peaks between 9°–10° and 16°–17° 2θ with Pearson VII functions.

3-D Geological Modeling

Twenty-eight original geological cross sections (for locations, see Fig. 1C) were used to build the 3-D basin geometry of the Scillato wedge-top basin and its pre-orogenic substratum. Geological cross sections were first reconstructed using Move software (Midland Valley, Glasgow, UK). From older to younger, the represented horizons are: top Mufara, top Scillato, top Crisanti, top Caltavuturo, and top Numidian Flysch, which describe the Imerese substratum, and top Castellana Sicula, top Terravecchia 1, and top Terravecchia 2–3, which refer to the wedge-top basin units.

The Imerese succession was modeled assuming a layer-cake geometry, as lateral heterogeneities of the pelagic facies in the study area can be neglected. Stratigraphic horizons and faults after a first check of consistency (e.g., no overlaps and intersections) were exported as pointsets (.dat file) and imported in Skua-Gocad software to construct a more-refined watertight 3-D geological model. A 3-D model is said to be water tight when every stratigraphic horizon is continuously defined over the area of interest and has clean intersections with lateral boundaries, faults, unconformities, or erosion surfaces (Caumon et al., 2004).

Only major faults with vertical displacements >500 m and longer than 3 km were exported. Smaller faults geometrically close and belonging to the same set were merged (e.g., faults bounding the Mount Cervi–Rocca di Sciara–Sclafani Bagni structure), in order to reduce the complexity of the model and its simulation time.

Stratigraphic horizons and faults were interpreted individually by Move software (e.g., Tanner et al., 2003) and simultaneously by the Skua software (Jayr et al., 2008). Skua technology is based upon the definition of stratigraphic horizons as values of a parametric function on a tetrahedral support (e.g., Frank et al., 2007). A chronostratigraphic scale was built using the selected horizons to guarantee that no horizon crossing occurred. The software offers the possibility to choose different types of geological boundary: conformable, unconformable, baselap, and erosive. Stratigraphic horizon tops for the Imerese unit were selected as conformable, whereas boundaries between the wedge-top horizon tops were selected as unconformable. A volume of interest (VOI = 26 × 38 × 8 km), which indicates the amount of three-dimensional space occupied by faults and horizons, was defined to include the interpreted structures. The first step in the 3-D model construction resulted in a fault network that interpolates the fault points and defines the branching relations of the various sets of faults. Once the VOI is split into fault blocks bounded by the interpreted faults, the horizons are constructed for each stratigraphic sequence. Horizons are defined as isovalues of a spatial varying function representing the stratigraphic time in the faulted blocks. As a consequence, horizon-fault definitions are consistent, and geometrical cuts on faults are clean. Building a watertight model is also a good test on the quality of the data. Whenever some data points are incorrectly interpreted, for example, if they are assigned to the wrong side of a fault, the resulting time function becomes geologically incorrect. Thus, consistently interpreting and building a watertight model represent the first step in the quality control of the resulting model.

RESULTS

Organic Matter Optical Analysis

Deformed Pre-Orogenic Substratum

Samples from the Mufara, Crisanti, and Numidian Flysch Formations provided suitable results for the organic matter optical analysis (Fig. 5). No significant variations in levels of thermal maturity and trend were recognized in the Mount Cervi–Rocca di Sciara–Sclafani Bagni structure. The Mufara Formation contains small maceral fragments (10–20 μm) that belong to the huminite-vitrinite and inertinite groups. R_o% values ranging between 0.82% and 0.94% (sites 28–24, Table 1) indicate middle-late mature stages of hydrocarbon generation. Organic matter in the Crisanti Formation is abundant and mainly made up of maceral fragments belonging to the huminite-vitrinite and inertinite groups. R_o% values of 0.68% and 0.74% (sites 22 and 23, Table 1) indicate early-middle mature stages of hydrocarbon generation. Organic matter in the Numidian Flysch is mainly made up of macerals that belong to the huminite-vitrinite and subordinately the inertinite groups. Vitrinite fragments, 30–60 μm in size, are typically fractured. Pyrite, either finely dispersed or in small globular aggregates, is locally present. R_o% values ranging between 0.40% and 0.57% indicate immature to early mature stages for hydrocarbon generation. In conclusion, the succession shows an increase in levels of thermal maturity as a function of stratigraphic age (Fig. 4).

Scillato Wedge-Top Basin

Organic matter dispersed in the Castellana Sicula and Terravecchia Formations is heterogeneous and mainly composed of macerals belonging to the huminite-vitrinite and subordinately to the inertinite groups. Pyrite, either finely dispersed or in small globular aggregates, is locally present, associated with both groups of macerals. The Castellana Sicula Formation (site 11, Table 1) has an R_o% value of 0.45%. The Terravecchia 1 member shows R_o% values of 0.38%–0.39% (sites 09–10, Table 1), and the Terravecchia 2–3 member displays R_o% values ranging between 0.42% and 0.47% (sites 04–08, Table 1). The Terravecchia 1b member has macerals with R_o% values between 0.33% and 0.47% (sites 01–03, Table 1). In particular, two samples (PA10 and PM22 in Fig. 4) show two separate clusters of R_o% values indicating both indigenous (0.33%–0.42%) and reworked (0.49%–0.55%) populations of vitrinite fragments.

The Castellana Sicula Formation and the Terravecchia 1 member are characterized by a thermal maturity increase as a function of stratigraphic age. On the contrary, the Terravecchia 2–3 and Terravecchia 1b are characterized by a reverse trend, showing an increase in R_o% values moving upward in the succession (Fig. 4), interpreted as due to reworked organic fragments. Generally, the entire succession experienced the immature stage of hydrocarbon generation (Fig. 5).

X-Ray Diffraction Analysis on Fine-Grained Sediments

Deformed Pre-Orogenic Substratum of the Scillato Wedge-Top Basin

XRD analysis of the Numidian Flysch and the Imerese succession is listed in Table 1. Clay mineral assemblages for the Mufara Formation (sites 24–28, Table 1) are mainly constituted by

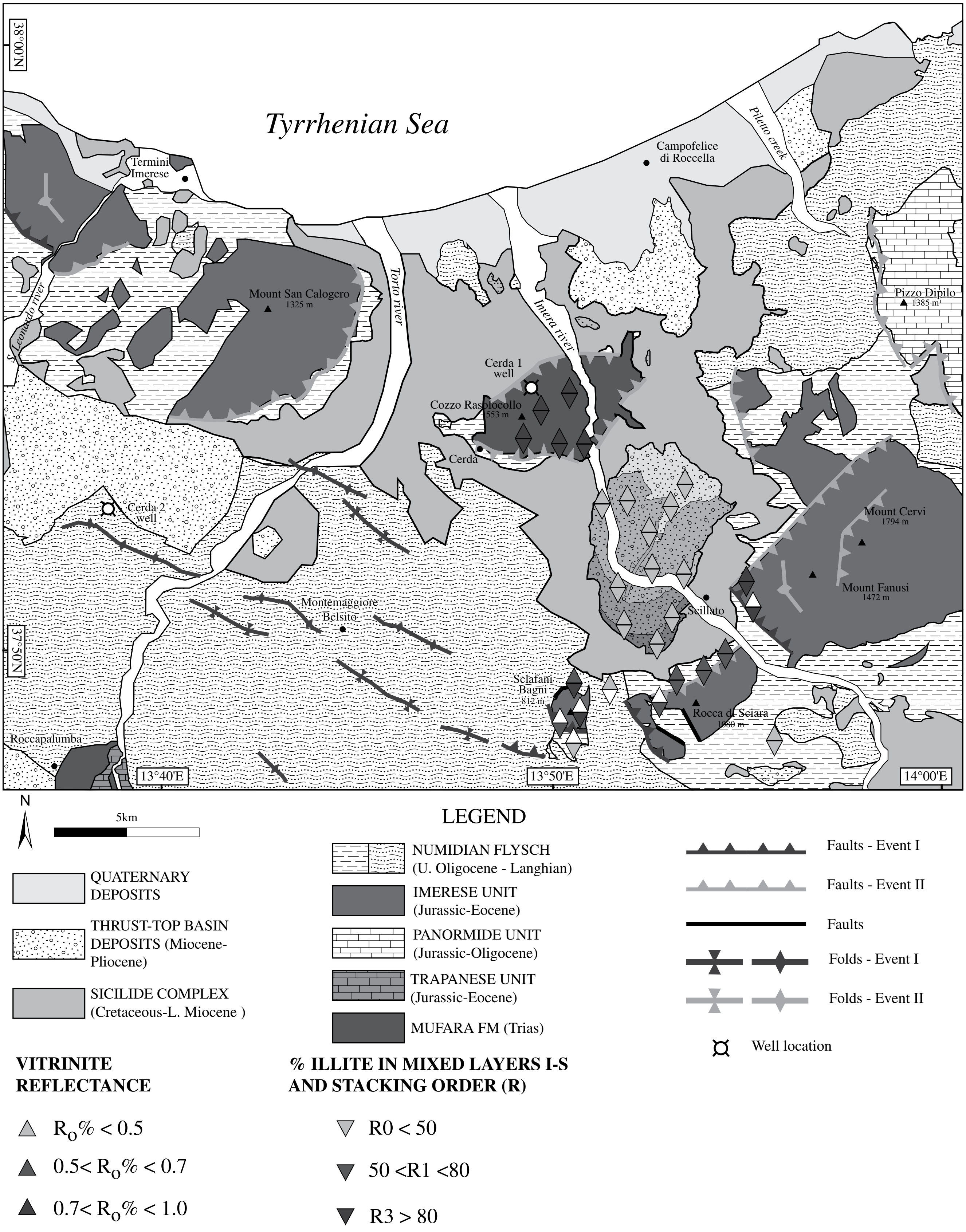

Figure 5. Map distribution of $R_o\%$ and illite content in mixed-layer illite-smectite (%I in I-S) and stacking order data. White triangles indicate no available data for the corresponding paleothermal parameter. U—Upper; L—Lower.

TABLE 1. ORGANIC MATTER MATURITY AND X-RAY DIFFRACTION DATA FOR THE SCILLATO WEDGE-TOP BASIN AND ITS PRE-OROGENIC SUBSTRATUM

Site	Sample	Latitude (°N)	Longitude (°E)	Formation	Age	R$_o$% (±s.d.)	X-ray analysis (<2 mm)	%I in I-S and stacking order	%C in C-S
01	PM22	37°53′12.78″	13°53′34.20″	Terravecchia 1b	Up. Tortonian–Low. Messinian	0.33 ± 0.04	I$_{26}$ I-S$_{24}$ K$_{40}$ Chl$_{10}$*	R0 40 + R1 78	
02	PM23	37°52′56.28″	13°53′16.55″	Terravecchia 1b	Up. Tortonian–Low. Messinian	0.42 ± 0.04	I$_{31}$ I-S$_{18}$ K$_{40}$ Chl$_{11}$*	R0 42 + R1 78	
03	PM28	37°52′37.18″	13°52′58.36″	Terravecchia 1b	Up. Tortonian–Low. Messinian	0.47 ± 0.05	I$_{24}$ I-S$_{21}$ K$_{43}$Chl$_{12}$*	R0 42 + R1 78	
04	PM29	37°53′4.24″	13°52′11.28″	Terravecchia 2-3	Up. Tortonian–Low. Messinian	0.46 ± 0.03	I$_{28}$ I-S$_{21}$ K$_{36}$ Chl$_{15}$*	R0 42 + R1 78	
05	PM25	37°51′58.04″	13°52′33.68″	Terravecchia 2-3	Up. Tortonian–Low. Messinian	0.44 ± 0.02	I$_{29}$ I-S$_{22}$ K$_{35}$ Chl$_{14}$*	R0 42 + R1 78	
06	PM14	37°53′13.90″	13°51′43.15″	Terravecchia 2-3	Up. Tortonian–Low. Messinian	0.47 ± 0.03	I$_{30}$ I-S$_{19}$ K$_{33}$ Chl$_{18}$*	R0 40 + R1 78	
07	PA10	37°51′35.30″	13°52′23.52″	Terravecchia 2-3	Up. Tortonian–Low. Messinian	0.42 ± 0.06	I$_{25}$ I-S$_{24}$ K$_{37}$ Chl$_{14}$*	R0 50 + R1 80	
08	PM18-19	37°51′44.71″	13°53′25.29″	Terravecchia 2-3	Up. Tortonian–Low. Messinian	0.42 ± 0.03	I$_{26}$ I-S$_{22}$ K$_{36}$ Chl$_{16}$	R0 45 + R1 70	
09	PA08	37°50′56.37″	13°52′42.47″	Terravecchia 1	Up. Tortonian–Low. Messinian	0.38 ± 0.05	I$_{28}$ I-S$_{24}$K$_{34}$Chl$_{14}$	R0 50 + R1 80	
10	MF5	37°50′58.33″	13°52′34.42″	Terravecchia 1	Up. Tortonian–Low. Messinian	0.39 ± 0.06	I$_{34}$ I-S$_{22}$K$_{38}$Chl$_{6}$	R0 50 + R1 80	
11	MF6	37°50′44.98″	13°53′14.10″	Castellana Sicula	Up. Serravallian–Low. Tortonian	0.45 ± 0.03	I$_{24}$ I-S$_{35}$ K$_{39}$ Chl$_{2}$	R0 50	
12	PA44	37°49′50.00″	13°51′49.20″	Numidian Flysch	Up. Oligocene–Low. Miocene	0.46 ± 0.05			
13	PA60	37°48′53.8″	13°55′36.8″	Numidian Flysch	Up. Oligocene–Low. Miocene	0.40 ± 0.07	I$_{9}$ I-S$_{14}$ K$_{73}$ Chl$_{4}$	R0 50 + R1 78	
14	PA43	37°48′44.40″	13°51′10.80″	Numidian Flysch	Up. Oligocene–Low. Miocene		I$_{7}$ I-S$_{10}$ K$_{83}$	R1 55	
15	PM35	37°50′22.40″	13°54′34.50″	Numidian Flysch	Up. Oligocene–Low. Miocene	0.57 ± 0.07	I$_{24}$ I-S$_{23}$ K$_{52}$ Chl$_{1}$*	R1 70	
16	PM34	37°50′3.51″	13°53′50.35″	Numidian Flysch	Up. Oligocene–Low. Miocene	0.54 ± 0.04	I$_{37}$ I-S$_{22}$ K$_{13}$ Chl$_{28}$*	R1 76	
17	MF4	37°49′52.81″	13°53′36.23″	Numidian Flysch	Up. Oligocene–Low. Miocene	0.57 ± 0.04	I$_{16}$ I-S$_{6}$ K$_{70}$ Chl$_{8}$	R1 72	
18	PA45	37°49′37.70″	13°53′36.23″	Caltavuturo	Up. Paleocene–Low. Oligocene		I$_{47}$ I-S$_{13}$ C-S $_{21}$ Chl$_{19}$	R1 78	80
19	PA41	37°49′4.40″	13°51′19.70″	Caltavuturo	Up. Paleocene–Low. Oligocene		I$_{20}$ I-S$_{19}$ C-S $_{32}$ Chl$_{29}$	R1 78	80
20	PA46	37°51′36.70″	13°54′50.60″	Crisanti	Up. Toarcian–Albian		I$_{72}$ I-S$_{12}$ Chl$_{16}$	R3 83	
21	PA40	37°49′13.80″	13°51′23.90″	Crisanti	Up. Toarcian–Albian		I$_{69}$ I-S$_{23}$ Chl$_{8}$	R3 83	
22	PA47	37°51′38.20″	13°54′52.20″	Crisanti	Up. Toarcian–Albian	0.74 ± 0.08	I$_{65}$ I-S$_{33}$ Chl$_{2}$	R3 85	
23	PA39	37°49′22.90″	13°51′23.30″	Crisanti	Up. Toarcian–Albian	0.68 ± 0.08	I$_{76}$ I-S$_{16}$ K$_{7}$ Chl$_{1}$	R3 86	
24	PM1	37°54′19.59″	13°50′39.61″	Mufara	Middle–Upper Carnian	0.83 ± 0.05	I$_{38}$ I-S$_{26}$ Chl$_{36}$	R3 86	
25	PM2	37°54′23.67″	13°51′10.38″	Mufara	Middle–Upper Carnian	0.82 ± 0.05	I$_{40}$ I-S$_{28}$ Chl$_{32}$*	R3 84	
26	PM6	37°54′37.82″	13°50′19.79″	Mufara	Middle–Upper Carnian	0.92 ± 0.04	I$_{44}$ I-S$_{37}$ C-S $_{13}$ K$_{3}$ Chl$_{3}$	R3 84	60
27	PM7	37°54′34.72″	13°49′59.63″	Mufara	Middle–Upper Carnian	0.83 ± 0.05	I$_{30}$ I-S$_{16}$ C-S $_{19}$ K$_{11}$Chl$_{24}$	R3 83	80
28	PM5	37°54′43.68″	13°50′30.19″	Mufara	Middle–Upper Carnian	0.94 ± 0.05	I$_{25}$ I-S$_{16}$ C-S $_{36}$ K$_{10}$ Chl$_{13}$*	R3 84	80

Note: R$_o$%—vitrinite reflectance; s.d.—standard deviation; I—illite; I-S—mixed-layer illite-smectite; C-S—mixed-layer chlorite-smectite; K—kaolinite; Chl—chlorite; R parameter—mixed-layer illite-smectite stacking order; %I in I-S—illite content in mixed-layer illite-smectite; %C in C-S—chlorite content in mixed-layer chlorite-smectite; Up.—Upper; Low.—Lower. Subscript numbers correspond to mineral weight percentage.

*Rectorite.

illite ranging from 25% to 44%, mixed-layer I-S (16%–37%), and chlorite (up to 36%). In the basal portion of the Mufara Formation (sites 26–28, Table 1), mixed-layer chlorite-smectite (13%–36%) and kaolinite (3%–11%) occur. The Crisanti Formation is characterized by illite (65%–76%), mixed-layer I-S (12%–33%), and subordinate amounts of chlorite. Kaolinite occasionally occurs in sample PA39 (site 23, Table 1). The Caltavuturo Formation (sites 18–19, Table 1) contains illite (20%–47%), mixed-layer I-S (13%–19%), chlorite-smectite (21%–32%), and chlorite (19%–29%). The Numidian Flysch (sites 13–17, Table 1) is mainly constituted by a kaolinite-rich assemblage with contents between 13% and 83% and subordinate amounts of illite (from 7% to 37%), mixed-layer I-S (6%–23%), and chlorite (up to 28%). XRD patterns of the Numidian Flysch and the Mufara Formation display the first-order superstructure reflection of rectorite (sites 15, 16, 25, and 28).

Random-ordered I-S (R0) with high expandability (50% of illite layers, which characterize the upper portion of the Numidian Flysch) converts into short-range ordered structures (R1) with an illite content of 55%–78% in the lower portion of the Numidian Flysch and Caltavuturo Formations (sites 12–19, Table 1) and evolves to long-range ordered structures (R3) in the Crisanti and Mufara Formations (sites 20–28, Table 1) with an illite content of 83%–86%. The Numidian Flysch and the Caltavuturo Formation experienced levels of thermal maturity consistent with early diagenetic conditions, whereas the Crisanti and Mufara Formations underwent deeper burial in late diagenesis (Merriman and Frey, 1999; Aldega et al., 2007).

Scillato Wedge-Top Basin

XRD analyses of the <2 μm grain-size fraction for the Terravecchia and Castellana Sicula Formations are shown in Table 1. The Castellana Sicula Formation (site 11, Table 1) is mainly constituted by mixed-layer illite-smectite (35%) and kaolinite (39%) and subordinate amounts of illite (24%). Chlorite does not exceed 2%. Mixed-layer I-S is composed of randomly ordered structures with an illite content of 50% (Fig. 5).

Terravecchia 1 member (sites 09–10, Table 1) is composed of kaolinite (36% mean value), illite (31% mean value), mixed-layer illite-smectite (23% mean value), and chlorite (10% mean value). Similar mineralogical assemblages and contents were observed in the Terravecchia 2–3 member (sites 04–08, Table 1), which is constituted by kaolinite (33%–37%), illite (25%–30%), mixed-layer illite-smectite (19%–24%), and chlorite (14%–18%). In the Terravecchia 1b member (sites 01–03, Table 1), kaolinite is the most abundant clay mineral, with contents up to 43%, followed by illite (24%–31%), mixed-layer illite-smectite (18%–24%), and chlorite (10%–12%).

Two populations of mixed-layer I-S with different compositions and stacking orders have been recorded in the Terravecchia Formation and have been interpreted as a mixture of diagenetic and inherited phases. I-S with no preferred sequence in stacking of layers (R0) shows a slight increase of illite content as a function of stratigraphic age from 40% to 50%, indicating burial diagenesis (Fig. 5), whereas short-range ordered I-S (R1) with illite contents of 70%–80% shows no correlation with depth and has been interpreted as an inherited phase. Both in the Terravecchia 2–3 and in the Terravecchia 1b members, XRD patterns show the first-order superstructure reflection (*d*-spacing: ~2.7 nm) that corresponds to mixed-layer clay minerals with alternating layer types of illite and smectite (rectorite).

3-D Geological Modeling

Reconstructed geological cross sections (Fig. 1C) were oriented both NE-SW (perpendicular to main thrust direction) and NW-SE (perpendicular to the high-angle transpressive fault direction) in order to build the 3-D model extrapolating thrusts and high-angle faults both laterally and at depth. The main constraint for depth came from the seismic reflection profile of the SI.RI.PRO (Sismica a Riflessione Profonda) project (Fig. 2). According to the seismic profile interpretation (Catalano et al., 2013), the Imerese unit reaches depths of 5–6 km. Thrust geometry and their lateral connections were reconstructed using field data and geological maps (Broquet, 1968; Mascle, 1979; Catalano et al., 2011; Gugliotta and Gasparo Morticelli, 2012; Barreca and Monaco, 2013). NE-dipping thrust sheets characterizing the Mount Cervi–Rocca di Sciara–Sclafani Bagni and the Mount San Calogero structures were exhumed and emergent due to the high-angle transpressive faults activity.

Between these structures and toward the SW, folds are observed showing the same orientation as the emerging thrusts (NW-SE) affecting the Numidian Flysch. Blind thrusts were interpreted and reconstructed at the base of these folds. Conversely, the thrust fault affecting the Lercara unit shows a different orientation (WNW-ESE).

Based on reconstructed cross sections, the geological model for the study area was first built using the Move software, which allowed us to obtain a 2.5-dimensional model (Fig. 6A), and then using Skua-Gocad software, which allowed us to reconstruct the 3-D geometry (Figs. 6B and 6C). The Move model allows two main fault sets with clear intersection relationships to be detected: (1) NW-SE–striking thrusts with southwestward tectonic transport (blue faults in Fig. 6A), and (2) NE-SW high-angle transpressive faults (red faults in Fig. 6A). The 3-D representation creates a geometrically consistent model, where seven major high-angle faults displace four main thrusts (Fig. 6B).

In general, NE-dipping thrusts (labeled N1, N3, and N4 in Fig. 6B) deform the Imerese succession and the Numidian Flysch, creating hanging-wall ramp open anticlines. The NNE-dipping thrust (N2 in Fig. 6B) branches against the N1 thrust and involves the Lercara unit. Thrust dip angles vary from almost zero along the basal detachment level (Mufara Formation) up to ~40° close to N1 thrust emergence (SW edge of Mount Cervi). These faults describe an imbricate thrust system (Boyer and Elliott, 1982). Reconstructed thrust displacement and dip angles increase toward the NE. In the southwestern sector, deformation is accommodated by major folds, and the Scillato wedge-top basin depocenter is located within the synform generated between the N1 and N3 thrusts (Fig. 6B).

High-angle faults (red faults in Fig. 6B) striking NE-SW are almost vertical and cut the pile of thin-skinned thrusts, involving deeper crustal levels. Fault displacement increases toward the NE across the Mount San Calogero and along the Mount Cervi–Rocca di Sciara–Sclafani Bagni structures, as shown in the official geological map of the area (Catalano et al., 2011). In the northeastern portion of the study area, the interaction between thrusts and high-angle faults generates a non-coaxial fold system (axes show two preferential distributions, NW-SE and NE-SW), which is recognized in the gentle dome of the Mount Cervi structure (Barreca and Monaco, 2013). The second fault set generates a main depocenter located between the Mount Cervi–Rocca di Sciara–Sclafani Bagni and the Mount San Calogero structures. The 3-D model in Figure 6C shows the geometry of the Scillato wedge-top basin, characterized by: (1) depocenter migration toward the north through time, recorded by the decreasing dip angles of the evolving Terravecchia Formation, from ~40° (Terravecchia 1 member) to ~10° (Terravecchia 1b member), and (2) a NNE-SSW–elongated synform.

DISCUSSION

Thermal Maturity of the Scillato Wedge-Top Basin and its Pre-Orogenic Substratum

Burial and thermal modeling of the Scillato wedge-top basin and its deformed substratum was carried out using Basin Mod (1996) 2-D software, calibrated against the indigenous population of vitrinite reflectance data and authigenic mixed-layer I-S. For this reason, we considered: a R_o% value of 0.45% and I% in mixed-layer I-S of 50% (site 11, Table 1) for the Castellana Sicula Formation; R_o% values ranging between 0.38 and 0.42 (sites 07–10, Table 1) and I% in I-S ranging between 40% and 50% (sites 04–10, Table 1) for the Terravecchia 1 and 2–3 members; and a R_o% value of 0.33% (site 01 in Table 1) and I% in I-S ranging between 40% and 42% (sites 01–03, Table 1) for the Terravecchia 1b member.

The main assumptions for modeling included the following: (1) the rock decompaction factors applied only to clastic deposits, according to the method of Sclater and Christie (1980); (2) sea-level changes were neglected, as thermal evolution is mainly affected by sediment thickness rather than by water depth (Butler, 1992); (3) thermal modeling was performed using the Lawrence Livermore National Laboratories (LLNL) Easy %Ro method based on Burnham and Sweeney (1989) and Sweeney and Burnham (1990); (4) thrusting was considered instantaneous when compared with the duration of sedimentation, as generally suggested by theoretical models (Endignoux and Wolf, 1990); (5) present-day heat flow of 60–70 mW m^{-2} was extracted from borehole data sets and available maps (GeoThopica [Banca Dati Nazionale Geotermica, Consiglio Nazionale delle Ricerche, http://geothopica.igg.cnr.it/]; Granath and Casero, 2004), whereas paleo–heat flow values were evaluated using the correlation between vitrinite reflectance and mixed-layer I-S data based on the kinetic model of vitrinite maturation of Burnham and Sweeney (1989) and the kinetics of the I-S reaction determined by Hillier et al. (1995); and (6) thickness, lithology, and age of sediments were obtained from geological maps (Broquet, 1968; Catalano et al., 2011).

Burial history reconstructed for the Scillato wedge-top basin (Fig. 7A) began during the late Serravallian with deposition of the Castellana Sicula marls (50 m), followed by the 1200-m-thick sequence of conglomerates, sandstones,

Figure 6. (A) Geological model reconstructed using Move software and constrained by original geological cross sections (for location, see Fig. 1C). Blue surfaces indicate thrusts related to the first tectonic event; red surfaces indicate high-angle transpressive faults related to the second tectonic event. Horizons representing tops of different formations are shown along the cross sections. (B) Three-dimensional (3-D) geological model extracted by Skua-Gocad software. The model to the left shows fault surfaces, where blue surfaces indicate thrusts, namely, N1, N2, N3, and N4, and red surfaces indicate high-angle transpressive faults. In the model to the right, horizons representing tops of formations and the locations of the Scillato wedge-top basin, Mount San Calogero and Cervi, preserved from erosion, are shown. (C) Detailed 3-D geological model for the Scillato wedge-top basin. Surfaces for the Castellana Sicula Formation and the Terravecchia members are reconstructed above the deformed substratum made up of the Sicilide Complex and Numidian Flysch.

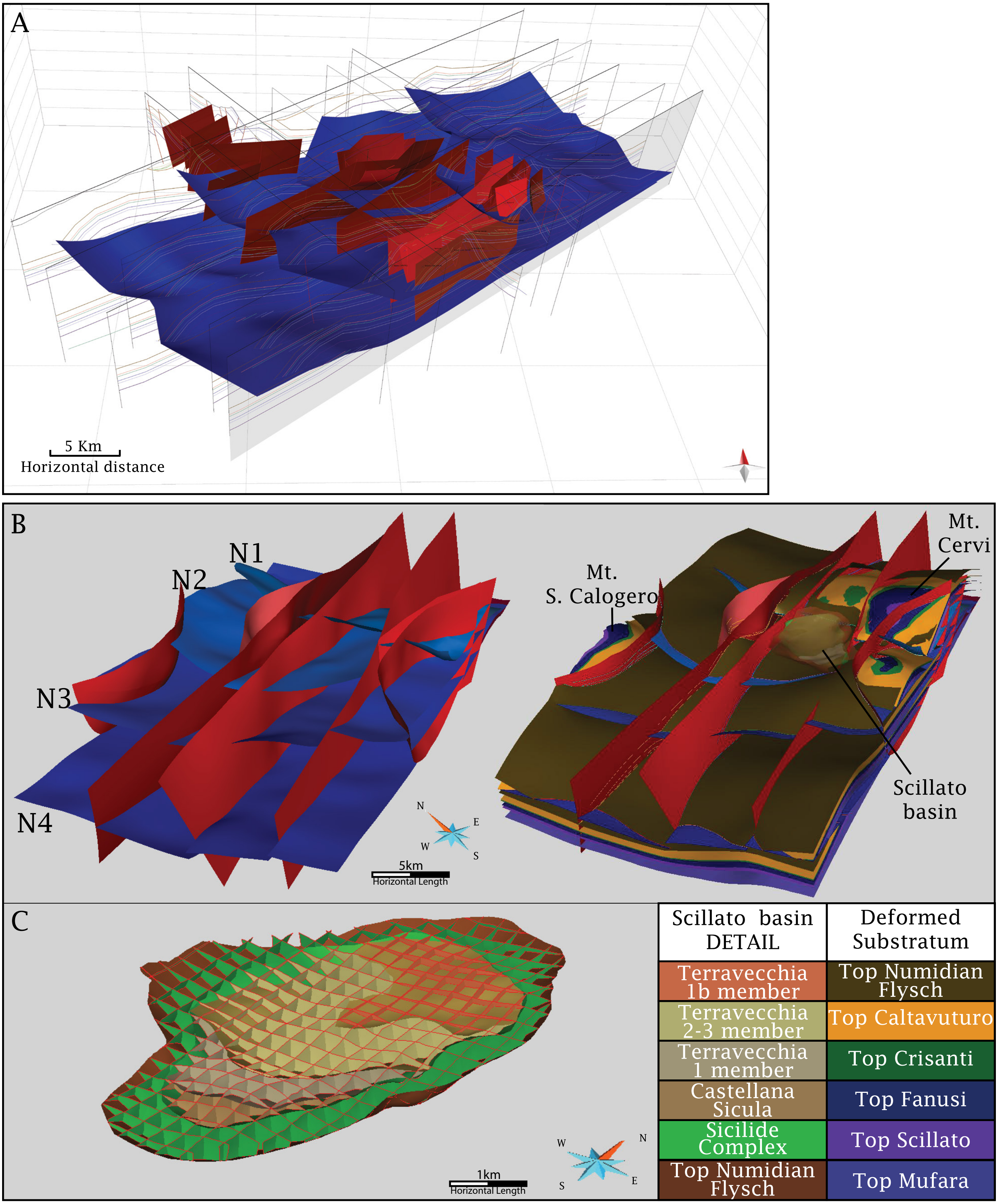
A
5 Km
Horizontal distance
B
N1
N2
N3
N4
N
E
W
S
5km
Horizontal Length
Mt.
S. Calogero
Mt.
Cervi
Scillato
basin
C
1km
Horizontal Length
W
N
S
E
Scillato basin DETAIL
Deformed Substratum
Terravecchia 1b member
Top Numidian Flysch
Terravecchia 2-3 member
Top Caltavuturo
Terravecchia 1 member
Top Crisanti
Castellana Sicula
Top Fanusi
Sicilide Complex
Top Scillato
Top Numidian Flysch
Top Mufara

Figure 6.

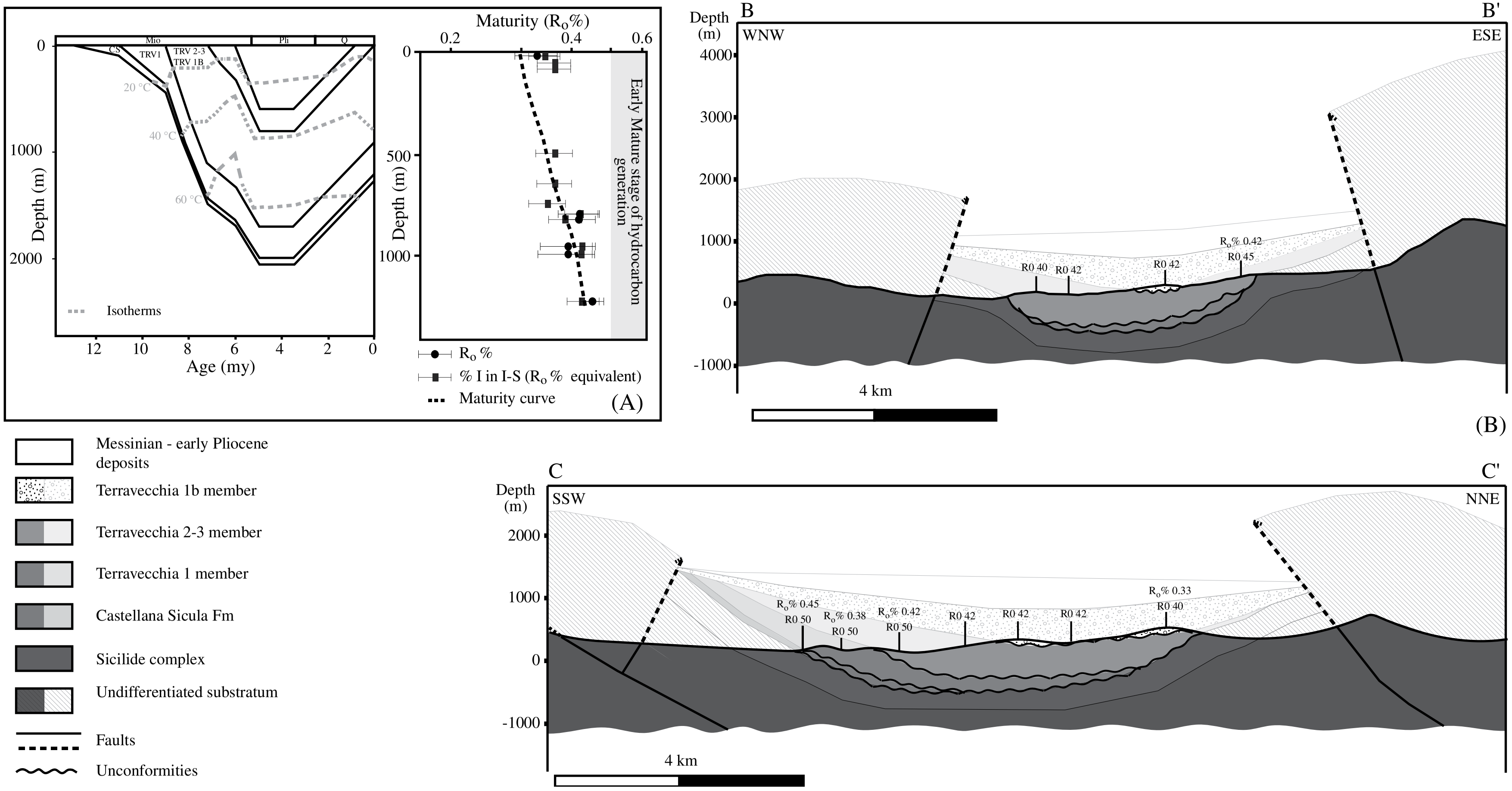

Figure 7. (A) Representative one-dimensional burial and thermal model of the Scillato wedge-top basin. (B) Original cross sections B-B′ and C-C′ (for location, see Fig. 3) with projected paleothermal data showing the thickness of the eroded strata calculated from thermal models. Shaded fills indicate the eroded formations. %I in I-S—illite content in mixed-layer illite-smectite; R_o%—vitrinite reflectance data; CS—Castellana Sicula Formation; TRV1—Terravecchia 1 member; TRV2–3, TRV1B—Terravecchia 2–3 and 1b members; Mio—Miocene; Pli—Pliocene; Q—Quaternary.

and claystones of the Terravecchia Formation during the Tortonian. A regional unconformity between the Castellana Sicula and Terravecchia Formations (Figs. 7B and C) marks a first episode of subaerial exposure. From the Messinian until the early Pliocene, deposition of gypsumarenites, calcarenites, and marls pertaining to the Gessoso-Solfifero Group and Trubi Formation occurred, with a minimum thickness of 800 m (Fig. 7). A comparable thickness of Messinian–Lower Pliocene deposits (~550 m) is exposed in the Ciminna wedge-top basin, located at ~20 km west of the Scillato wedge-top basin (see Fig. 1C; Gugliotta et al., 2014).

Thermal modeling shows a maximum sedimentary burial of ~2 km for the base of the Castellana Sicula Formation during Messinian–early Pliocene time and related maximum temperature of 78 °C (Fig. 7A). Exhumation started during the late Pliocene after the end of the Trubi Formation deposition, and erosion removed ~0.8 km of sediments (Fig. 7).

The reconstructed evolution for the Imerese unit began during the Middle Triassic with the deposition of claystones, sandstones, and limestones of the Mufara Formation and continued until the earliest Oligocene with the deposition of limestones, dolostones, calcilutites, and marls of the Scillato, Fanusi, Crisanti, and Caltavuturo Formations (Fig. 8A). During the Oligocene, a depositional hiatus occurred, associated with the end of carbonate sedimentation and the onset of the Numidian Flysch deposition. Modeled sedimentary thickness for the Numidian Flysch is ~1.3 km. During the Serravallian, the Imerese unit and Numidian Flysch were incorporated into the advancing orogenic wedge (Gugliotta et al., 2014) and stacked up into thrust sheets buried by ~0.8 km of more internal units (made up of part of the Numidian Flysch and Sicilide units). At that time, the base of the Imerese unit along the Mount Cervi–Rocca di Sciara–Sclafani Bagni structure experienced maximum burial to a depth of ~3.5 km with maximum temperatures of ~150 °C (Fig. 8). From the latest Tortonian, exhumation of the Imerese unit occurred (Fig. 8), driven by activity of high-angle faults (Event II in Fig. 3). U-Th/He dating on apatite crystals was tentatively performed on samples from the Mufara and Numidian Flysch Formations in order to obtain quantitative constraints for the exhumation age of the Imerese unit. Unfortunately, very few (three crystals for the Numidian Flysch and one for the Mufara Formation) and highly broken apatite crystals (<60 μm of diameters) were separated. Only two apatite grains from the Numidian Flysch (site 15, Fig. 3) provided reliable results, indicating different ages for their closure temperature: 113.94 ± 2.7 Ma and 5.13 ± 0.22 Ma (M. Zattin, 2017, personal commun.). The older age clearly indicates an inherited apatite grain, as it is older than the Numidian Flysch stratigraphic age, whereas the Pliocene age could refer to the exhumation phase of the Imerese unit, and this indication was taken into account in the performed models. Nevertheless, the small number of crystals and the wide age interval did not allow a statistical analysis of the results (Reiners and Ehlers, 2005).

Evolutionary Scenarios for the Lercara Unit

A different tectonic evolutionary scenario is proposed for the Lercara unit, because its origin and emplacement mechanism are still a matter of debate. In the Mount Rasolocollo–Cerda area, the Mufara Formation is surrounded by the Numidian Flysch and the Sicilide Complex with a contact of uncertain nature. For the Mufara Formation, R_o% values ranging from 0.82% to 0.94% and R3 I-S with an illite content of 83%–86% indicate levels of thermal maturity consistent with the late mature stage of hydrocarbon generation. The Numidian Flysch in surrounding areas shows random-ordered (R0) and/or short-range ordered I-S (R1) and R_o% values ranging from 0.40% to 0.57%, indicating lower levels of thermal maturity, in the immature to early mature stages of hydrocarbon generation. Thus, a gap in levels of thermal maturity is observed between the two formations.

Three evolutionary scenarios may be consistent with this present-day configuration. Nevertheless, geological features, and mineralogical and paleothermal data allow us to discriminate the most likely among them. Such scenarios differ in amount of burial, timing, and mode of structural thickening and exhumation.

In the first model (Fig. 9), the Lercara unit represents an extensional structural high developed in earliest Jurassic time and inherited during chain building. In this scenario, after the sedimentation of the Mufara Formation (1.4 km), only a few meters of sediments of the Imerese succession were deposited on it until the early Oligocene (Fig. 9A). During Oligocene–Langhian times, in front of the orogenic wedge, a foredeep developed on top of this structure, and an ~1.3-km-thick succession of the Numidian Flysch was deposited. Shallow-seated thrusts developed after the Serravallian, as a consequence of the advancing orogenic wedge, leading to tectonic thickening of the foredeep deposits and the emplacement of the Sicilide Complex onto the Numidian Flysch (Fig. 9A). Subsequently, the Castellana Sicula Formation was deposited (~0.2 km) onto the deformed substratum in a wedge-top setting until the end of the Serravallian. At that time, the Mufara Formation experienced its maximum burial to 4.2 km, in agreement with thermal modeling constrained by paleothermal data (Fig. 9B). In the latest Tortonian, the onset of the activity of high-angle transpressive faults (Event II) uplifted the area, leading to the erosion of 3.2 km of the Tertiary to Triassic units (Fig. 9B). This process led to the exhumation of the Mufara Formation, where the Numidian Flysch currently lies stratigraphically on top of the structural high and locally on the footwall of transpressive faults (Fig. 9A).

This scenario is consistent with 3.2 km of exhumation of the Lercara high (located NW of Scillato wedge-top basin), whereas only 1.8 km of exhumation occurred for the Mount Cervi–Rocca di Sciara–Sclafani Bagni high (located SE of Scillato wedge-top basin; Fig. 8). These amounts of exhumation are not supported by paleocurrent directions reconstructed for the Scillato wedge-top basin, which indicate a main source area for the wedge-top sediments located to the east and southeast (Gugliotta and Gasparo Morticelli, 2012; Gugliotta et al., 2013), where low exhumation amounts have been calculated.

In the second model (Fig. 10), the Lercara unit experienced continuous deposition of pelagic facies deposits of the Imerese succession (~2 km) in a passive-margin setting until Langhian time, and of Numidian Flysch in foredeep facies. After the Serravallian, the advancing orogenic wedge induced the development of shallow-seated thrusts, which led to the emplacement of thin thrust sheets made up of the Sicilide Complex (~0.3 km) onto the Numidian Flysch (Figs. 10A and 10B). The Castellana Sicula Formation was deposited (~0.2 km) in a wedge-top setting onto this deformed substratum. From latest Tortonian time, high-angle transpressive fault activity drove the exhumation of the Mufara Formation, resulting in 2.65 km of erosion (Fig. 10B) and the present-day configuration where Triassic deposits tectonically overlie the younger Numidian Flysch succession (Fig. 10A). Also, in this scenario, mean paleocurrent directions do not support the exhumation amounts depicted in the previous scenario.

In the third scenario (Fig. 11), the Lercara unit experienced two different phases of exhumation. Continuous sedimentation of the Imerese succession occurred until the early Eocene in a passive-margin setting, and the Mufara Formation experienced maximum burial of ~2.35 km at that time (Fig. 11A). During the Oligocene, an early orogenic low-angle normal fault removed 1.35 km of the Triassic–Eocene succession, inducing isostatic footwall rebound responsible for the exhumation of the Mufara Formation (Figs. 11A and 11B). Subsequently, the Numidian Flysch was deposited both on the

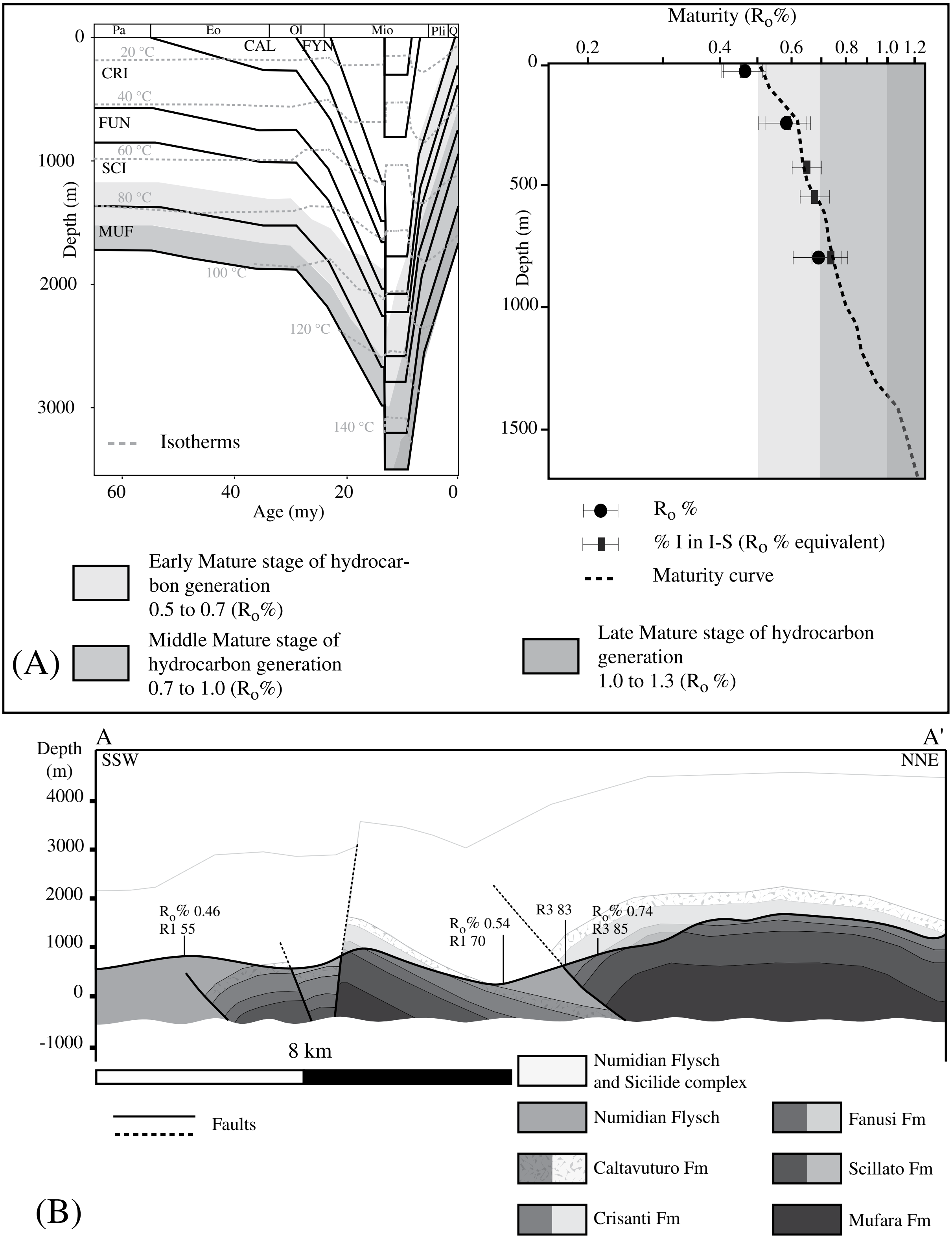

Figure 8. (A) Representative one-dimensional burial and thermal model for the Imerese unit in the last 60 m.y. (B) Original cross section A-A′ (for location, see Fig. 3) with projected paleothermal data showing the thickness of the eroded strata. Shaded fills indicate the eroded formations. %I in I-S—illite content in mixed-layer illite-smectite; R_o%—vitrinite reflectance data; MUF—Mufara Formation; SCI—Scillato Formation; FUN—Fanusi Formation; CRI—Crisanti Formation; CAL—Caltavuturo Formation; FYN—Numidian Flysch; Pa—Paleocene; Eo—Eocene; Ol—Oligocene; Mio—Miocene; Pli—Pliocene; Q—Quaternary.

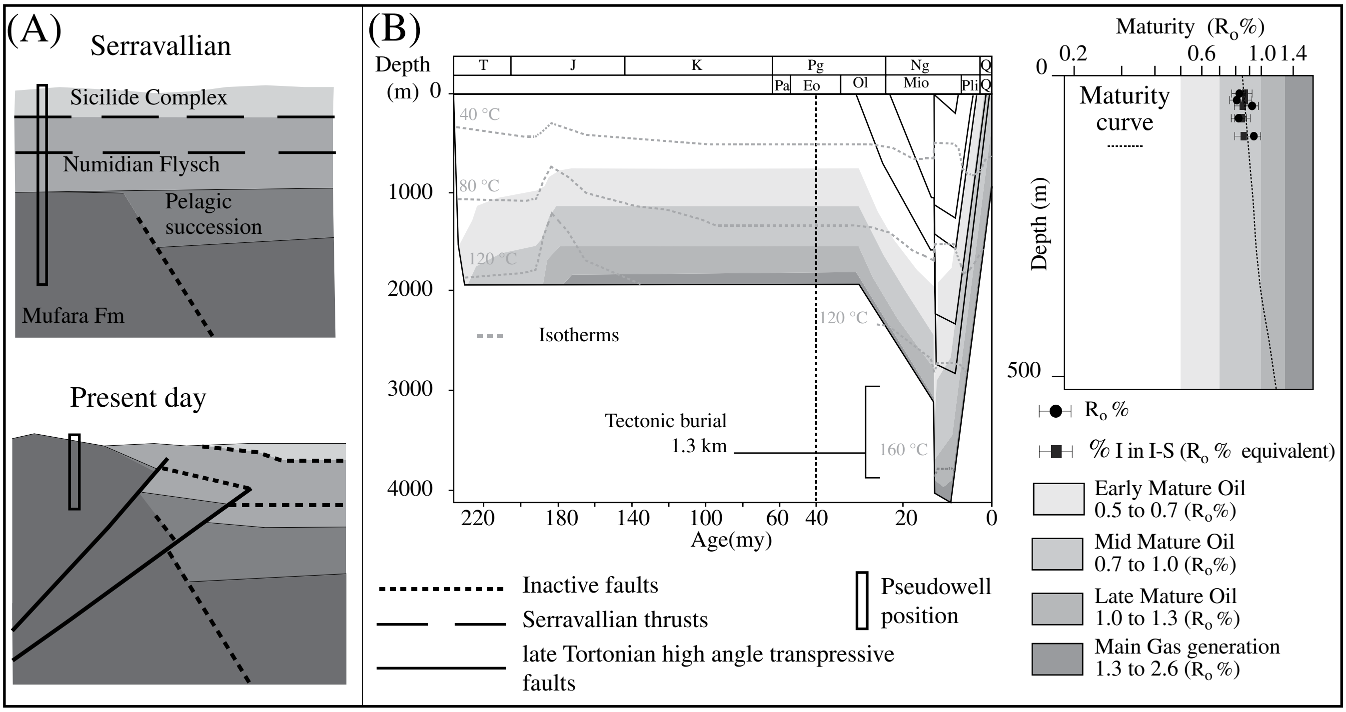

Figure 9. (A) Simplified tectonic sketches showing Serravallian and present-day setting for the Lercara unit, considered as a structural high within the Imerese basin (not to scale). (B) Representative one-dimensional (pseudo-well) burial and thermal model for the Lercara unit. %I in I-S—illite content in mixed-layer illite-smectite; R_o%—vitrinite reflectance data. T—Triassic; J—Jurassic; K—Cretaceous; Pg—Paleogene; Ng—Neogene; Q—Quaternary. See Figure 8 caption for other abbreviations.

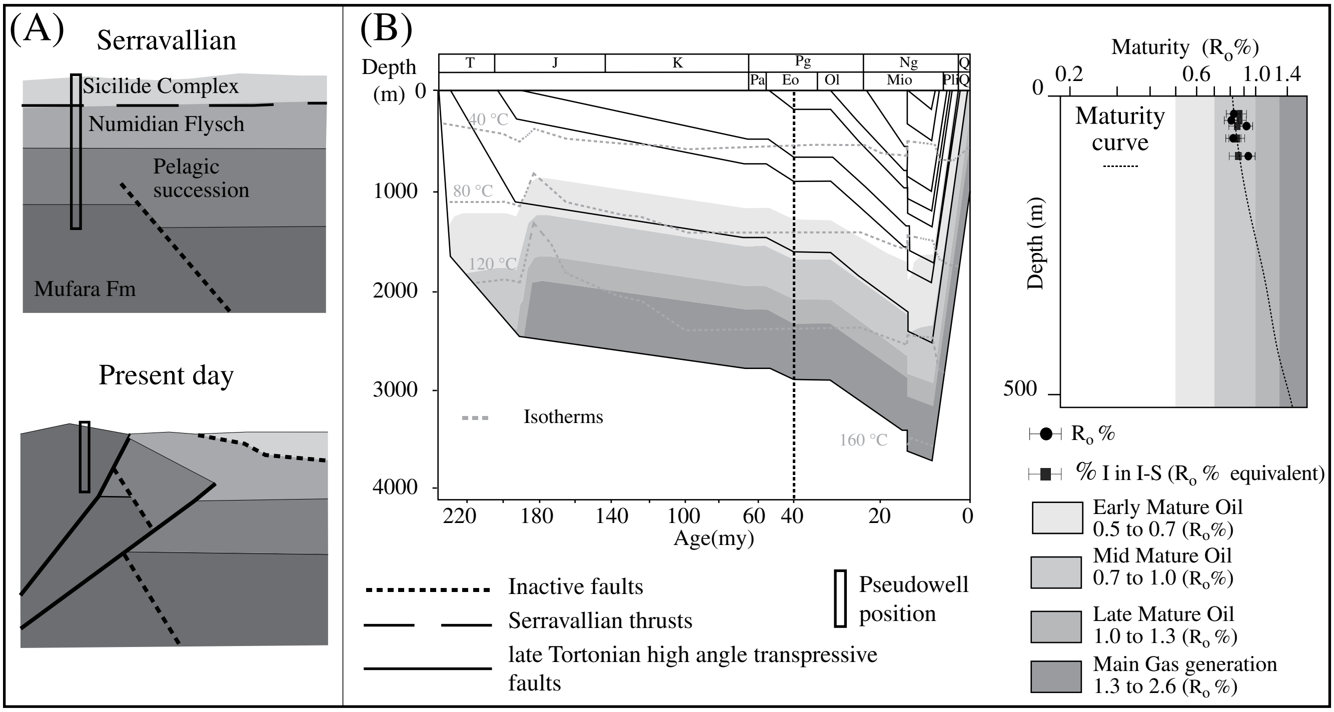

Figure 10. (A) Simplified tectonic sketches showing Serravallian and present-day setting where the Lercara unit succession is considered as the base of the Imerese succession (not to scale). (B) Representative one-dimensional (pseudo-well) burial and thermal model for the Lercara unit. %I in I-S—illite content in mixed layers illite-smectite; R_o%—vitrinite reflectance data; See Figures 8 and 9 captions for other abbreviations.

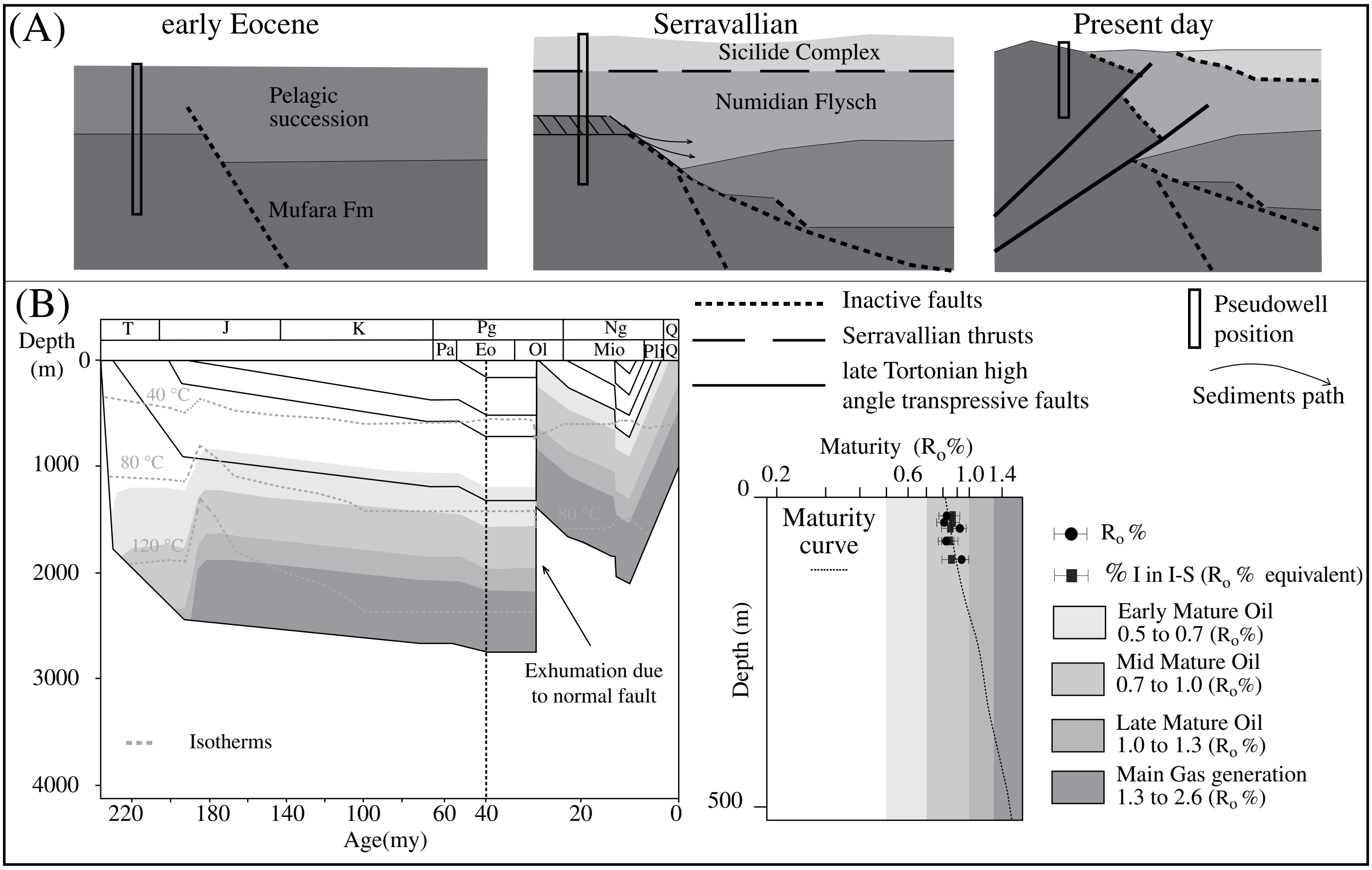

Figure 11. (A) Simplified tectonic sketches showing early Eocene, Serravallian, and present-day setting for the Lercara unit considering a low-angle normal fault acting during the Oligocene (not to scale). (B) Representative one-dimensional (pseudo-well) burial and thermal model for the Lercara unit. %I in I-S—illite content in mixed-layer illite-smectite; R_o%—vitrinite reflectance data. See Figures 8 and 9 for other abbreviations.

hanging-wall and footwall blocks with changing thickness. In the hanging wall, where the Numidian Flysch is thicker, it was locally fed by the erosion of the Mufara Formation. During the Serravallian, the Sicilide Complex (0.3 km thick) was thrust over the Numidian Flysch, followed by deposition of the Castellana Sicula Formation (0.1 km), burying the Mufara Formation to a depth of 2.2 km (Fig. 11B). Beginning in the latest Tortonian, final exhumation occurred, driven by high-angle transpressive faults (Event II), resulting in 1.2 km of erosion (Figs. 11A and 11B).

This scenario is consistent with the distribution of paleocurrent directions and XRD analyses of the <2 µm grain-size fraction of sediments. In detail, the mineralogical assemblage of the substratum units highlights the occurrence of rectorite both in the Mufara Formation and in the Numidian Flysch (Table 1), suggesting that the Mufara Formation was exhumed in the Oligocene, partially feeding the Numidian Flysch.

Source-to-Sink System: Insights into the Kinematic Evolution of the Belt

Paleothermal indicators, coupled with sedimentological and structural data (Gugliotta and Gasparo Morticelli, 2012; Gugliotta et al., 2013), allow us to describe the evolution of a source (deformed substratum) to sink (wedge-top) system for the Scillato Basin, identifying two main source areas feeding the wedge-top basin since Serravallian time.

The basal part of the wedge-top basin succession (Castellana Sicula Formation and Terravecchia 1 member) shows depocenter migration toward the NW (Event I), coherent with the main thrust transport direction to the SW and subsequent deformation as a result of activity of the NE-SW–directed transpressive faults during Event II (Figs. 6B and 6C). The latter event generated an approximately NE-SW–trending asymmetric synform where the top of the succession (Terravecchia 2–3 and 1b members, late Tortonian) is accommodated (Fig. 6C).

The Terravecchia 1 member contains pebbles mainly made up of igneous and metamorphic rocks, indicating a continental source area for sediments filling the basin. According to paleocurrent reconstruction, the source area was located to the NW of the Scillato basin, and pebbles belong to the European domain, most likely Sardinia and Kabilo-Calabride crystalline basement (Gugliotta and Gasparo Morticelli, 2012; Gugliotta et al., 2013). The sandy-shaly portion of the Terravecchia 1 member contains indigenous fragments of organic matter and two populations of mixed-layer phases. The population with low expandable mixed-layer I-S (R1 80%) represents the inherited fraction of sediments probably coming from the dismantling of the Numidian Flysch that was exhumed during Serravallian–Tortonian times in more internal areas, originally located to the NW (Di Paolo et al., 2014).

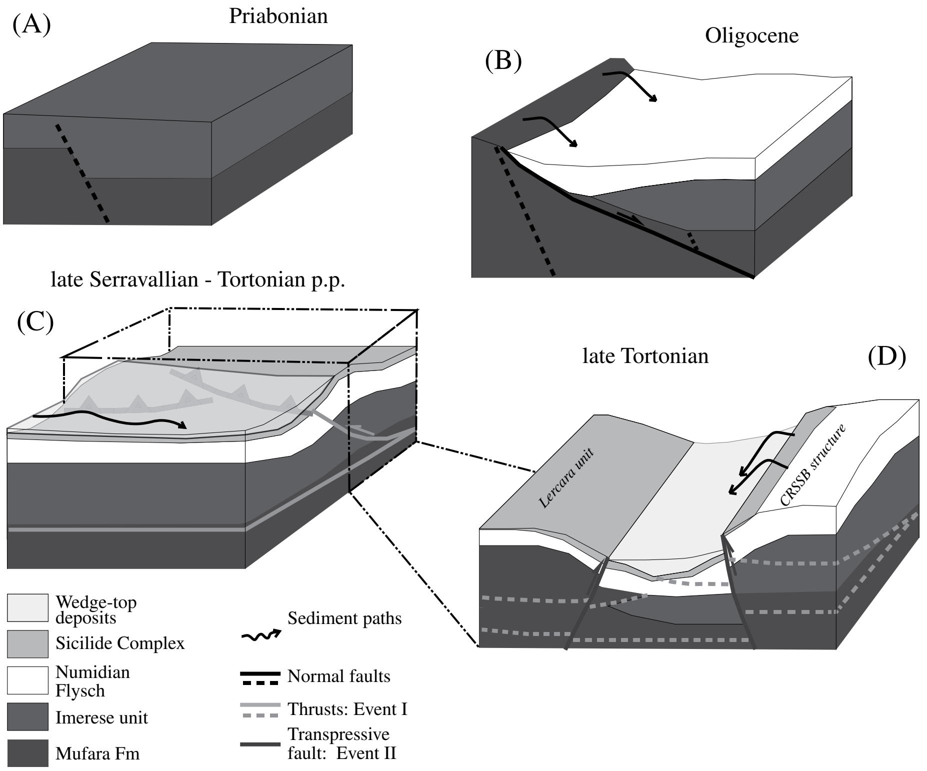

Figure 12. Tectonic evolutionary model for the Sicilian fold-and-thrust belt (not to scale). (A) Passive-margin setting during the late Eocene. (B) Low-angle extensional tectonics generating exhumation of the Upper Triassic Mufara Formation, which fed the Numidian Flysch during the Oligocene. (C) Thin-skinned thrust tectonics affecting the Imerese unit and onset of wedge-top basin sedimentation in late Serravallian–Tortonian times. (D) High-angle transpressive faults driving exhumation of the Imerese unit and controlling wedge-top basin deposition during the latest Tortonian. Dotted lines indicate inactive faults. CRSSB structure—Mount Cervi–Rocca di Sciara–Sclafani Bagni structure.

A different source area fed the late Tortonian deposits of the Terravecchia 2–3 and 1b members. They contain high amounts of reworked organic and inorganic material. The inorganic fraction of sediments displays minerals coming from the Scillato Basin margins, such as mixed-layer I-S with high illite content (R1 70%–80%) and rectorite, which represent the detrital minerals filling the basin during the late Tortonian. Such a mineralogical assemblage has been detected in the Numidian Flysch succession exposed to the SE of the Scillato wedge-top basin along the Mount Cervi–Rocca di Sciara–Sclafani Bagni structure that has been exhuming since the late Tortonian (Fig. 8). Reworked vitrinite macerals also show R_o% values between 0.42% and 0.55%, similar to those measured for the Numidian Flysch (0.40%–0.57%) from surrounding areas, strengthening this hypothesis. In addition, paleocurrent analysis identified a source area for sediments during the latest Tortonian located to the SE of the Scillato wedge-top basin, corresponding to the Mount Cervi–Rocca di Sciara–Sclafani Bagni structure (Gugliotta and Gasparo Morticelli, 2012) and consistent with the detrital mineral supply identified by XRD analysis.

Coupling paleothermal and mineralogical data with 1-D thermal and 3-D geological modeling of both the Scillato wedge-top basin and its substratum, a new kinematic evolutionary scenario for this part of the Sicilian fold-and-thrust belt can be proposed (Fig. 12). From the Triassic to the early Eocene, passive-margin conditions led to the deposition of the Imerese succession. Jurassic normal faults probably generated horst and graben structures (Fig. 12A). In the Oligocene, early orogenic low-angle extensional faults developed in the foreland region, detaching the Triassic–Eocene section of the Imerese succession from the Mufara Formation (Fig. 12B). Isostatic footwall rebound led the Mufara Formation to be exhumed, partially providing clasts and detrital minerals to the Numidian Flysch deposited in the hanging-wall block. As a result, the hanging-wall block corresponds to the Mount Cervi–Rocca di Sciara–Sclafani Bagni structure where the Numidian Flysch is 1.8 km thick, and the footwall block corresponds to the Lercara unit where the Numidian Flysch is 0.4 km thick.

We interpret such low-angle normal faulting in the Sicilian fold-and-thrust belt as a result of early orogenic extension occurring during the Oligocene in the foreland region and anticipating the onset of contractional deformation. At that time, in more internal areas to the NW, the Peloritani Mountains were already involved in the tectonic wedge, recording a first phase of exhumation (Thomson, 1994; Aldega et al., 2011; Di Paolo et al., 2014).

Early orogenic normal faulting in the Central and Northern Apennines has been interpreted by several authors as the response to flexural bending of the lithosphere (e.g., peripheral bulge; Bradley and Kidd, 1991; Doglioni, 1995; Tavani et al., 2015, and reference therein) and has been highlighted by field evidence and imaged in seismic cross sections (Tavarnelli and Peacock, 1999; Scisciani et al., 2002; Mirabella et al., 2004; De Paola et al., 2006; Carminati et al., 2014). These faults differ from similar extensional structures that triggered exhumation in the adjacent Southern Apennines part of the same orogen (Corrado et al., 2005; Mazzoli et al., 2006, 2008) and also controlled the development of early wedge-top basins (Vitale et al., 2011; Ciarcia et al., 2012; Corrado et al., 2019). In fact, these latter faults were induced at shallow crustal levels by gravitational readjustment within the tectonic wedge associated with thick-skinned shortening at depth during orogen building (e.g., Mazzoli et al., 2008).

Beginning in Serravallian time, the advancing orogenic wedge generated shallow-seated thrusts that brought the Sicilide Complex to thrust over the Numidian Flysch and deformed the Imerese substratum succession (Figs. 6B and 12C). At that time, sediment fluxes moved parallel to the main thrust direction (NW-SE), indicating a main source area for sediments located to the NW of the Scillato Basin. As a result, the Castellana Sicula Formation and Terravecchia 1 member were deposited in a wedge-top setting. Since latest Tortonian time, high-angle transpressive faults have cut the shallow-seated thrusts (Fig. 6B), leading to the differential exhumation of the Imerese unit along the Mount Cervi–Rocca di Sciara–Sclafani Bagni structure (Fig. 8A) and the Lercara unit in the Rasolocollo-Cerda area (Fig. 12D). At that time, a shift in source area for sediments from NW to E-ESE is recorded by the Terravecchia 2–3 and Terravecchia 1b members, which were mainly fed by the erosion of the Sicilide Complex and Numidian Flysch located along the Mount Cervi–Rocca di Sciara–Sclafani Bagni structure.

CONCLUSIONS

The burial and thermal history of the Scillato wedge-top basin and its pre-orogenic substratum allows us to define levels of thermal maturity in the Triassic to Tortonian succession of the Sicilian fold-and-thrust belt. The wedge-top basin fill experienced shallow burial (~2 km) and levels of thermal maturity in the immature stage of hydrocarbon generation and early diagenesis, whereas the pre-orogenic substratum experienced a maximum burial of 3.5 km in deep diagenetic conditions.

The integration of mineralogical and paleothermal data with 1-D thermal and 3-D geological modeling allowed us to reconstruct the Scillato wedge-top basin geometry and evolution through time in the framework of a source-to-sink system, unraveling the kinematic evolution of the Apennine-Maghrebian fold-and-thrust belt. In particular, low-angle normal faulting occurred during early orogenic extension predating contractional deformation.

ACKNOWLEDGMENTS

We are indebted for highly stimulating discussions on Sicilian tectonics and structural evolution of fold-and-thrust belts with Giuseppe Cadel, Jean Letouzey, Rob Butler, Dominique Frizon De Lamotte, Mauro Agate, and Luca Basilone. We also greatly thank Massimiliano Barchi for helping us in the first stage of this research and for valuable discussions on the evolution of the African passive margin that inspired some of the evolutionary scenarios proposed in this paper. Warm thanks are due to Massimiliano Zattin for providing facilities for apatite separation and U-Th/He analysis. Analytical facilities for organic matter and clay mineral analyses were available at the Academic Laboratory of Basin Analysis (ALBA) at Roma Tre University. Thermal and structural modeling was performed by means of different software packages available both at Roma Tre University (Italy) and IFPen (France) thanks to Platte Rivers (1D B-mod), Midland Valley (Move), and Paradigm (Skua-Gocad) temporary licenses. IFPen is also kindly acknowledged for hosting Balestra for a 5 mo at Rueil-Malmaison (France) during her Ph.D. project. Funding was provided by: Italian Ministry of Education, University and Research (MIUR) to Dottorato in Scienze della Terra, University Roma Tre, XXXI cycle (coordinator: Claudio Faccenna); IFPen funding for Ph.D. student stage program; and Sveva Corrado "Roma Tre" Research Funding. Moreover, the Grant of Excellence Departments, MIUR (ARTICOLO 1, COMMI 314–337 LEGGE 232/2016), is gratefully acknowledged. We are grateful to the associate editor, an anonymous reviewer, and D.K. Muirhead for detailed revisions and helpful suggestions.

REFERENCES CITED

Aldega, L., Corrado, S., Grasso, M., and Maniscalco, R., 2007, Correlation of diagenetic data from organic and inorganic studies in the Apenninic-Maghrebian fold-and-thrust belt: A case study from eastern Sicily: The Journal of Geology, v. 115, no. 3, p. 335–353, https://doi.org/10.1086/512756.

Aldega, L., Corrado, S., Di Paolo, L., Somma, R., Maniscalco, R., and Balestrieri, M.L., 2011, Shallow burial and exhumation of the Peloritani Mts. (NE Sicily, Italy): Insight from paleo-thermal and structural indicators: Geological Society of America Bulletin, v. 123, p. 132–149, https://doi.org/10.1130/B30093.1.

Aldega, L., Carminati, E., Scharf, A., Mattern, F., and Al-Wardi, M., 2017, Estimating original thickness and extent of the Semail ophiolite in the eastern Oman Mountains by paleothermal indicators: Marine and Petroleum Geology, v. 84, p. 18–33, https://doi.org/10.1016/j.marpetgeo.2017.03.024.

Aldega, L., Bigi, S., Carminati, E., Trippetta, F., Corrado, S., and Kavoosi, M.A., 2018, The Zagros fold-and-thrust belt in the Fars Province (Iran): II. Thermal evolution: Marine and Petroleum Geology, v. 93, p. 376–390, https://doi.org/10.1016/j.marpetgeo.2018.03.022.

Allen, P.A., 2008, From landscapes into geological history: Nature, v. 451, p. 274–276, https://doi.org/10.1038/nature06586.

Allen, P.A., and Allen, J.R., 2013, Basin Analysis: Principle and Application to Petroleum Play Assessment (3rd ed.): Oxford, UK, Wiley-Blackwell, 619 p.

Avellone, G., and Barchi, M.R., 2003, Le pieghe minori nelle Unità Imeresi e Trapanesi dei Monti di Palermo e il loro significato nell-evoluzione tettonica dell-area: Bollettino della Società Geologica Italiana, v. 122, p. 277–294.

Avellone, G., Barchi, M.R., Catalano, R., Gasparo Morticelli, M., and Sulli, A., 2010, Interference between shallow and deep-seated structures in the Sicilian belt, Italy: Journal of the Geological Society [London], v. 167, p. 109–126, https://doi.org/10.1144/0016-76492008-163.

Balsamo, F., Aldega, L., De Paola, N., Faoro, I., and Storti, F., 2014, The signature and mechanics of earthquake ruptures along shallow creeping faults in poorly lithified sediments: Geology, v. 42, no. 5, p. 435–438, https://doi.org/10.1130/G35272.1.

Barnes, J.B., and Heins, W.A., 2008, Plio-Quaternary sediment budget between thrust belt erosion and foreland deposition in the central Andes, southern Bolivia: Basin Research, v. 21, p. 91–109.

Barreca, G., and Monaco, C., 2013, Vertical-axis rotation in the Sicilian belt: New structural constrains from the Madonie Mts. (Sicily, Italy): Italian Journal of Geosciences, v. 132, p. 407–421, https://doi.org/10.3301/IJG.2012.44.

Basilone, L., Frixa, A., Trincianti, E., and Valenti, V., 2016, Permian–Cenozoic deep-water carbonate rocks of the Southern Tethyan Domain. The case of central Sicily: Italian Journal of Geosciences, v. 135, no. 2, p. 171–198, https://doi.org/10.3301/IJG.2015.07.

Basin Mod® 1-D for Windows™, 1996, A Basin Analysis Modeling System, Version 5.4 Software: Denver, Colorado, Platte River Associates, 386 p.

Bello, M., Franchino, A., and Merlini, S., 2000, Structural model of eastern Sicily: Memorie della Societa Geologica Italiana, v. 55, p. 61–70.

Bianchi, F., Carbone, S., Grasso, M., Invernizzi, G., Lentini, F., Longaretti, G., Merlini, S., and Mostardini, F., 1989, Sicilia orientate: Profilo geologico Nebrodi-Iblei: Memorie della Società Geologica Italiana, v. 38, p. 429–458.

Boyer, S.E., and Elliott, D., 1982, Thrust system: American Association of Petroleum Geologists Bulletin, v. 66, p. 1196–1230.

Bradley, D.C., and Kidd, W.S.F., 1991, Flexural extension of the upper continental crust in collisional foredeeps: Geological Society of America Bulletin, v. 103, no. 11, p. 1416–1438, https://doi.org/10.1130/0016-7606(1991)103<1416:FEOTUC>2.3.CO;2.

Broquet, P., 1968, Etude Géologique de la Région des Madonies (Sicile) [Ph.D. thesis]: Lille, France, Université de Lille, 553 p.

Burnham, A.K., and Sweeney, J.J., 1989, A chemical kinetic model of vitrinite maturation and reflectance: Geochimica et Cosmochimica Acta, v. 53, p. 2649–2657, https://doi.org/10.1016/0016-7037(89)90136-1.

Bustin, R.M., Barnes, M.A., and Barnes, W.C., 1990, Determining levels of organic diagenesis in sediments and fossil fuels, *in* McIleareath, I.A., and Morrow, D.W., eds., Diagenesis: St. John's, Canada, Geoscience Canada Reprint, 4th series, p. 205–226.

Butler, R.W.H., 1992, Hydrocarbon maturation, migration and tectonic loading in the western Alps, *in* England, W.A., and Fleet, A.J., eds., Petroleum Migration: Geological Society of London Special Publication 59, p. 227–244.

Butler, R.W.H., and Grasso, M., 1993, Tectonic controls on base-level variations and depositional sequences within thrust-top and foredeep basins: Examples from the Neogene thrust belt of central Sicily: Basin Research, v. 5, p. 137–151, https://doi.org/10.1111/j.1365-2117.1993.tb00062.x.

Caputo, M., Panza, G.F., and Postpischl, D., 1970, Deep structure of the Mediterranean Basin: Journal of Geophysical Research, v. 75, p. 4919–4923, https://doi.org/10.1029/JB075i026p04919.

Caricchi, C., Aldega, L., and Corrado, S., 2015, Reconstruction of maximum burial along the Northern Apennines thrust wedge (Italy) by indicators of thermal exposure and modeling: Geological Society of America Bulletin, v. 127, p. 428–442, https://doi.org/10.1130/B30947.1.

Carminati, E., Fabbi, S., and Santantonio, M., 2014, Slab bending, syn-subduction normal faulting, and out-of-sequence thrusting in the Central Apennines: Tectonics, v. 33, no. 4, p. 530–551, https://doi.org/10.1002/2013TC003386.

Catalano, R., and D'Argenio, B., 1982, Schema geologico della Sicilia occidentale, *in* Catalano, R., and D'Argenio, B., eds., Guida Alla Geologia della Sicilia Occidentale: Guide Geologiche Regionali: Memorie della Societa Geologica Italiana, Supplement A, v. 24, p. 9–41.

Catalano, R., D'Argenio, B., and Torelli, L., 1989, From Sardinia Channel to Sicily Straits. A geologic section based on seismic and field data, *in* Boriani, A., et al., eds., The Lithosphere in Italy: Advances in Earth Science Research: Rome, Accademia Nazionale dei Lincei, Atti dei Convegni Lincei, v. 80, p. 109–27.

Catalano, R., Di Stefano, P., and Kozur, H., 1991, Permian circum-Pacific deep-water faunas from the Western Tethys (Sicily, Italy)—New evidence for the position of the Permian Tethys: Palaeogeography, Palaeoclimatology, Palaeoecology, v. 87, p. 75–108, https://doi.org/10.1016/0031-0182(91)90131-A.

Catalano, R., Di Stefano, P., Sulli, A., and Vitale, F.P., 1996, Paleogeography and structure of the Central Mediterranean: Sicily and its offshore area: Tectonophysics, v. 260, p. 291–323, https://doi.org/10.1016/0040-1951(95)00196-4.

Catalano, R., Franchino, A., Merlini, S., and Sulli, A., 2000, Central western Sicily structural setting interpreted from seismic reflection profiles: Memorie della Società Geologica Italiana, v. 55, p. 5–16.

Catalano, R., Avellone, G., Basilone, L., Contino, A., Agate, M., Gugliotta, C., Di Maggio, C., Di Stefano, E., Gennaro, C., Arnone, M., Sulli, A., Di Maio, D., Mancuso, M., Abate, B., and Gasparo Morticelli, M., 2011, Note Illustrative della Carta Geologica d'Italia alla Scala 1:50.000 Sheets 609–596 "Termini Imerese–Capo Plaia," con Allegata Carta Geologica in scala 1:50.000 (2a): Istituto Superiore per la Protezione e la Ricerca Ambientale (ISPRA), Servizio Geologico d'Italia, scale 1:50,000.

Catalano, R., Valenti, V., Albanese, C., Accaino, F., Sulli, A., Tinivella, U., Gasparo Morticelli, M., Zanolla, C., and Giustiniani, M., 2013, Sicily's fold/thrust belt and slab rollback: The SI.RI.PRO. seismic crustal transect: Journal of the Geological Society [London], v. 170, p. 451–464, https://doi.org/10.1144/jgs2012-099.

Catalano, S., De Guidi, G., Romagnoli, G., Torrisi, S., Tortorici, G., and Tortorici, L., 2008, The migration of plate boundaries in SE Sicily: Influence on the large-scale kinematic model of the African promontory in southern Italy: Tectonophysics, v. 449, p. 41–62, https://doi.org/10.1016/j.tecto.2007.12.003.

Caumon, G., Lepage, F., Sword, C.H., and Mallet, J.L., 2004, Building and editing a sealed geological model: Mathematical Geology, v. 36, no. 4, p. 405–424, https://doi.org/10.1023/B:MATG.0000029297.18098.8a.

Channell, J.E.T., Catalano, R., and D'Argenio, B., 1980, Paleomagnetism and deformation of the Mesozoic continental margin of Sicily: Tectonophysics, v. 61, p. 391–407, https://doi.org/10.1016/0040-1951(80)90242-5.

Channell, J.E.T., Oldow, J.S., Catalano, R., and D'Argenio, B., 1990, Paleomagnetically determined rotations in the western Sicilian fold and thrust belt: Tectonics, v. 9, p. 641–660, https://doi.org/10.1029/TC009i004p00641.

Ciarcia, S., Mazzoli, S., Vitale, S., and Zattin, M., 2012, On the tectonic evolution of the Ligurian accretionary complex in southern Italy: Geological Society of America Bulletin, v. 124, p. 463–483, https://doi.org/10.1130/B30437.1.

Cifelli, F., and Mattei, M., 2010, Curved orogenic systems in the Italian peninsula: A paleomagnetic review: Journal of Virtual Explorer, v. 36, p. 1–23, https://doi.org/10.3809/jvirtex.2010.00239.

Corrado, S., Di Bucci, D., Naso, G., Giampaolo, C., and Adatte, T., 1998, Application of organic matter and clay mineral studies to the tectonic history of the Abruzzo-Molise-Sannio area, Central Apennines, Italy: Tectonophysics, v. 285, no. 1-2, p. 167–181, https://doi.org/10.1016/S0040-1951(97)00195-9.

Corrado, S., Aldega, L., Di Leo, P., Giampaolo, C., Invernizzi, C., Mazzoli, S., and Zattin, M., 2005, Thermal maturity of the axial zone of the Southern Apennines fold-and-thrust belt (Italy) from multiple organic and inorganic indicators: Terra Nova, v. 17, p. 56–65, https://doi.org/10.1111/j.1365-3121.2004.00584.x.

Corrado, S., Aldega, L., Balestrieri, M.L., Maniscalco, R., and Grasso, M., 2009, Structural evolution of the sedimentary accretionary wedge of the Alpine system in eastern Sicily: Thermal and thermochronological constraints: Geological Society of America Bulletin, v. 121, p. 1475–1490, https://doi.org/10.1130/B26420.1.

Corrado, S., Aldega, L., and Zattin, M., 2010, Sedimentary vs. tectonic burial and exhumation along the Apennines (Italy): Journal of Virtual Explorer, v. 36, https://doi org/10.3809/jvirtex.2010.00232.

Corrado, S., Aldega, L., Perri, F., Critelli, S., Muto, F., Schito, A., and Tripodi, V., 2019, Detecting synorogenic extension and sediment provenance of the Cilento wedge-top basin (Southern Apennines, Italy): Mineralogy and geochemistry of fine-grained sediments and petrography of dispersed organic matter: Tectonophysics, v. 750, p. 404–418, https://doi.org/10.1016/j.tecto.2018.10.027.

DeCelles, P.G., and Giles, K.A., 1996, Foreland basin systems: Basin Research, v. 8, p. 105–123, https://doi.org/10.1046/j.1365-2117.1996.01491.x.

De Paola, N., Mirabella, F., Barchi, M.R., and Burchielli, F., 2006, Early orogenic normal faults and their reactivation during thrust belt evolution: The Gubbio fault case study, Umbria-Marche Apennines (Italy): Journal of Structural Geology, v. 28, no. 11, p. 1948–1957, https://doi.org/10.1016/j.jsg.2006.06.002.

Dercourt, J., Zonenshain, L.P., Ricou, L.E., Kazmin, V.G., Le Pichon, X., Knipper, A.L., Grandjacquet, C., Sbortshikov, I.M., Geyssant, J., Lepvrier, C., Pechersky, D.H., Boulin, J., Sibuet, J.C., Savostin, L.A., Sorokhtin, O., Westphal, M., Bazhenov, M.L., Lauer, J.P., and Biju-Duval, B., 1986, Geologic evolution of the Tethys belt from the Atlantic to the Pamirs since the Lias: Tectonophysics, v. 123, p. 241–315, https://doi.org/10.1016/0040-1951(86)90199-X.

Dewey, J.F., Helman, M.L., Turco, E., Hutton, D.H.W., and Knott, S.D., 1989, Kinematics of the Western Mediterranean, *in* Coward, M.P., ed., Alpine Tectonics: Geological Society of London Special Publication 45, p. 265–283.

Di Paolo, L., Aldega, L., Corrado, S., and Mastalerz, M., 2012, Maximum burial and unroofing of Mt. Judica recess area in Sicily: Implication for the Apenninic–Maghrebian wedge dynamics: Tectonophysics, v. 530, p. 193–207, https://doi.org/10.1016/j.tecto.2011.12.020.

Di Paolo, L., Olivetti, V., Corrado, S., Aldega, L., Balestrieri, M.L., and Maniscalco, R., 2014, Detecting the stepwise propagation of the eastern Sicily thrust belt (Italy): Insight from thermal and thermochronological constraints: Terra Nova, v. 26, p. 363–371, https://doi.org/10.1111/ter.12106.

Di Stefano, P., and Gullo, M., 1997, Permian deposits of Sicily: A review: Geodiversitas, v. 19, no. 2, p. 193–202.

Di Stefano, P., McRoberts, C., Renda, P., Tripodo, A., Torre, A., and Torre, F., 2012, Middle Triassic (Ladinian) deep-water sediments in Sicily: New findings from the Madonie Mountains: Rivista Italiana di Paleontologia e Stratigrafia, v. 118, p. 235–246.

Doglioni, C., 1995, Geological remarks on the relationships between extension and convergent geodynamic settings: Tectonophysics, v. 252, p. 253–267, https://doi.org/10.1016/0040-1951(95)00087-9.

Doglioni, C., Harabaglia, P., Merlini, S., Mongelli, F., Peccerillo, A., and Piromallo, C., 1999, Orogens and slab vs. their direction of subduction: Earth-Science Reviews, v. 45, p. 167–208, https://doi.org/10.1016/S0012-8252(98)00045-2.

Endignoux, L., and Wolf, S., 1990, Thermal and kinematic evolution of thrust basins: A 2D numerical model, *in* Letouzey, J., ed., Petroleum Tectonics in Mobile Belts: Paris, Edit. Technip, p. 181–192.

Faccenna, C., Funiciello, F., Giardini, D., and Lucente, F.P., 2001, Episodic back-arc extension during restricted mantle convection in the Central Mediterranean: Earth and Planetary Science Letters, v. 187, p. 105–116, https://doi.org/10.1016/S0012-821X(01)00280-1.

Faccenna, C., Piromallo, C., Crespo-Blanc, A., Jolivet, L., and Rosetti, F., 2004, Lateral slab deformation and the origin of the Western Mediterranean arcs: Tectonics, v. 23, TC1012, https://doi.org/10.1029/2002TC001488.

Finetti, I.R., Lentini, F., Carbone, S., Del Ben, A., Di Stefano, A., Forlin, E., Guarnieri, P., Pipan, M., and Prizzon, A., 2005, Geological outline of Sicily and lithospheric tectono-dynamics of its Tyrrhenian margin from new CROP seismic data, *in* Finetti, I.R., ed., CROP PROJECT: Deep Seismic Exploration of the Central Mediterranean and Central Italy: Amsterdam, Netherlands, Elsevier, p. 319–375.

Flügel, E., Di Stefano, P., and Senowbari-Daryan, B., 1991, Microfacies and depositional structure of allochthonous carbonate base-of-slope deposits: The Late Permian Pietra di Salomone megablock, Sosio valley (western Sicily): Facies, v. 25, p. 147–186, https://doi.org/10.1007/BF02536758.

Frank, T., Tertois, A.-L., and Mallet, J.-L., 2007, 3-D reconstruction of complex geological interfaces from irregularly distributed and noisy point data: Computers & Geosciences, v. 33, no. 7, p. 932–943, https://doi.org/10.1016/j.cageo.2006.11.014.

Garver, J.J., Brandon, M.T., Roden-Tice, M., and Kamp, P.J.J., 1999, Exhumation history determined by detrital fission-track thermochronology, *in* Ring, U., Brandon, M.T., Lister, G.S., and Willett, S.D., eds., Exhumation Processes: Normal Faulting, Ductile Flow and Erosion: Geological Society of London Special Publication 154, p. 283–304, https://doi.org/10.1144/GSL.SP.1999.154.01.13.

Gasparo Morticelli, M., Valenti, V., Catalano, R., Sulli, A., Agate, M., Avellone, G., Albanese, C., Basilone, L., and Gugliotta, C., 2015, Deep controls on foreland basin system evolution along the Sicilian fold and thrust belt: Bulletin de la Société Géologique de France, v. 186, p. 273–290, https://doi.org/10.2113/gssgfbull.186.4-5.273.

Giunta, G., Nigro, F., and Renda, P., 2000, Extensional tectonics during Maghrebides chain building since late Miocene: Examples from northern Sicily: Annales Societatis Geologorum Poloniae, v. 70, p. 81–98.

Granath, J., and Casero, P., 2004, Tectonic setting of the petroleum systems in Sicily, *in* Swennen, R., Roure, F., and Granath, J., eds., Deformation, Fluid Flow and Reservoir Appraisal in Foreland Fold-and-Thrust Belts: American Association of Petroleum Geologists Hedberg Volume 1, p. 391–411.

Grasso, M., 2001, The Apenninic–Maghrebian orogen in southern Italy, Sicily and adjacent areas: Tectonophysics, v. 343, p. 135–163.

Grasso, M., Manzoni, M., and Quintili, A., 1987, Misure magnetiche sui Trubi della Sicilia orientale: Possibili implicazioni stratigrafiche e strutturali: Memorie della Società Geologica Italiana, v. 38, p. 459–474.

Guarnieri, P., 2004, Structural evidence for deformation by block rotation in the context of transpressive tectonics, northwestern Sicily (Italy): Journal of Structural Geology, v. 26, p. 207–219, https://doi.org/10.1016/S0191-8141(03)00102-0.

Gugliotta, C., 2012, Inner vs. outer wedge-top depozone "sequences" in the late Miocene (late Tortonian–early Messinian) Sicilian foreland basin system; new data from the Terravecchia Formation of NW Sicily: Journal of Geodynamics, v. 55, p. 41–55, https://doi.org/10.1016/j.jog.2011.11.002.

Gugliotta, C., and Gasparo Morticelli, M., 2012, Using high-resolution stratigraphy and structural analysis to constrain polyphase tectonics in wedge-top basins: Inferences from the late Tortonian Scillato Basin (central–northern Sicily): Sedimentary Geology, v. 273–274, p. 30–47, https://doi.org/10.1016/j.sedgeo.2012.06.009.

Gugliotta, C., Agate, M., and Sulli, A., 2013, Sedimentology and sequence stratigraphy of wedge-top clastic successions: Insights and open questions from the Upper Tortonian Terravecchia Formation of the Scillato Basin (central–northern Sicily, Italy): Marine and Petroleum Geology, v. 43, p. 239–259, https://doi.org/10.1016/j.marpetgeo.2013.02.004.

Gugliotta, C., Gasparo Morticelli, M., Avellone, G., Agate, M., Barchi, M.R., Albanese, C., Valenti, V., and Catalano, R., 2014, Middle Miocene–early Pliocene wedge-top basins of NW Sicily (Italy): Constraints for the tectonic evolution of a "non-conventional" thrust belt, affected by transpression: Journal of the Geological Society [London], v. 171, p. 211–226, https://doi.org/10.1144/jgs2013-009.

Hillier, S., Màtyàs, J., Matter, A., and Vasseur, G., 1995, Illite/smectite diagenesis and its variable correlation with vitrinite reflectance in the Pannonian Basin: Clays and Clay Minerals, v. 43, p. 174–183, https://doi.org/10.1346/CCMN.1995.0430204.

Izquierdo-Llavall, E., Aldega, L., Cantarelli, V., Corrado, S., Gil-Peña, I., Invernizzi, C., and Casas-Sainz, A., 2013, On the origin of cleavage in the central Pyrenees: Structural and paleo-thermal study: Tectonophysics, v. 608, p. 303–318, https://doi.org/10.1016/j.tecto.2013.09.027.

Jayr, S., Gringarten, E., Tertois, A.L., Mallet, J.L., and Dulac, J.C., 2008, The need for a correct geological modelling support: The advent of the UVT-transform: First Break, v. 26, p. 73–79.

Jolivet, M., Labaume, P., Monie, P., Brunel, M., Arnaud, N., and Campani, M., 2007, Thermochronology constraints for the propagation sequence of the south Pyrenean basement thrust system (France-Spain): Tectonics, v. 26, TC5007, https://doi.org/10.1029/2006TC002080.

Kozur, H.W., Krainer, K., and Mostler, H., 1996, Ichnology and sedimentology of the Early Permian deep-water deposits from the Lercara-Roccapalumba area (western Sicily, Italy): Facies, v. 34, p. 123–150, https://doi.org/10.1007/BF02546160.

Mascle, G.H., 1979, Etude géologique es Monts Sicanis, Sicile: Rivista Italiana di Paleontologia e Stratigrafia, v. XVI, p. 1–431.

Mazzoli, S., Aldega, L., Corrado, S., Invernizzi, C., and Zattin, M., 2006, Pliocene–Quaternary thrusting, synorogenic extension and tectonic exhumation in the Southern Apennines (Italy): Insights from the Monte Alpi area, *in* Mazzoli, S., and Butler, R.W.H., eds., Styles of Continental Contraction: Geological Society of America Special Paper 414, p. 55–77, https://doi.org/10.1130/2006.2414(04).

Mazzoli, S., D'Errico, M., Aldega, L., Corrado, S., Invernizzi, C., Shiner, P., and Zattin, M., 2008, Tectonic burial and "young" (<10 Ma) exhumation in the Southern Apennines fold-and-thrust belt (Italy): Geology, v. 36, no. 3, p. 243–246, https://doi.org/10.1130/G24344A.1.

Merriman, R.J., and Frey, M., 1999, Patterns of very low-grade metamorphism in metapelitic rocks, *in* Frey, M., and Robinson, D., eds., Low Grade Metamorphism:

Oxford, UK, Blackwell, p. 61–107, https://doi.org/10.1002/9781444313345.ch3.

Michael, N.A., Carter, A., Whittaker, A.C., and Allen, P.A., 2014, Erosion rates in the source region of an ancient sediment routing system: Comparison of depositional volumes with thermochronometric estimates: Journal of the Geological Society [London], v. 171, p. 401–412, https://doi.org/10.1144/jgs2013-108.

Mirabella, F., Ciaccio, M.G., Barchi, M.R., and Merlini, S., 2004, The Gubbio fault (central Italy): Geometry, displacement distribution and tectonic evolution: Journal of Structural Geology, v. 26, p. 2233–2249, https://doi.org/10.1016/j.jsg.2004.06.009.

Miuccio, G., Frixa, A., and Bertamoni, M., 2000, The Trapanese structural domain in the Termini Imerese Mountain area (Sicily): Memorie della Società Geologica Italiana, v. 55, p. 227–234.

Moore, D.M., and Reynolds, R.C., Jr., 1997, X-Ray Diffraction and the Identification and Analysis of Clay Minerals: Oxford, UK, Oxford University Press, 378 p.

Monaco, C., and De Guidi, G., 2006, Structural evidence for Neogene rotations in the eastern Sicilian fold and thrust bel: Journal of Structural Geology, v. 28, p. 561–574, https://doi.org/10.1016/j.jsg.2006.01.010.

Nigro, F., and Renda, P., 1999, Evoluzione geologica ed assetto strutturale della Sicilia centro settentrionale: Bollettino della Società Geologica Italiana, v. 118, p. 375–388.

Nigro, F., and Renda, P., 2000, Un modello di evoluzione tettono-sedimentaria dell'avanfossa Neogenica Siciliana: Bollettino della Società Geologica Italiana, v. 119, p. 1913–1930.

Ogniben, L., 1960, Nota illustrativa dello schema geologico della Sicilia nordorientale: Rivista Mineraria Siciliana, v. 64–65, p. 183–222.

Oldow, J.S., Channell, J.E.T., Catalano, R., and D'Argenio, B., 1990, Contemporaneous thrusting and large-scale rotations in the western Sicilian fold and thrust belt: Tectonics, v. 9, p. 661–681, https://doi.org/10.1029/TC009i004p00661.

Pinter, P.R., Butler, R.W.H., Hartley, A.J., Maniscalco, R., Baldassini, N., and Di Stefano, A., 2016, The Numidian of Sicily revisited: A thrust-influenced confined turbidite system: Marine and Petroleum Geology, v. 78, p. 291–311, https://doi.org/10.1016/j.marpetgeo.2016.09.014.

Reiners, P.W., and Ehlers, T.A., eds., 2005, Low-Temperature Thermochronology: Techniques, Interpretations, and Applications: Mineralogical Society of America and Geochemical Society, Reviews in Mineralogy and Geochemistry 58, 622 p., https://pubs.geoscienceworld.org/rimg/issue/58/1.

Roure, F., Howell, D.G., Muller, C., and Moretti, I., 1990, Late Cenozoic subduction complex of Sicily: Journal of Structural Geology, v. 12, p. 259–266, https://doi.org/10.1016/0191-8141(90)90009-N.

Schito, A., Andreucci, B., Aldega, L., Corrado, S., Di Paolo, L., Zattin, M., Szaniawski, R., Jankowski, L., and Mazzoli, S., 2018, Burial and exhumation of the western border of the Ukrainian Shield (Podolia): A multidisciplinary approach: Basin Research, v. 30, p. 532–549, https://doi.org/10.1111/bre.12235.

Scisciani, V., Tavarnelli, E., and Calamita, F., 2002, The interaction of extensional and contractional deformations in orogenic belts: The example of the Central Apennines, Italy: Journal of Structural Geology, v. 24, p. 1647–1658, https://doi.org/10.1016/S0191-8141(01)00164-X.

Sclater, J.G., and Christie, P.A.F., 1980, Continental stretching: An explanation of post–mid-Cretaceous subsidence on the central North Sea Basin: Journal of Geophysical Research, v. 85, p. 3711–3739, https://doi.org/10.1029/JB085iB07p03711.

Sømme, T.O., Helland-Hansen, W., Martinsen, O.J., and Thurmond, J.B., 2009, Relationships between morphological and sedimentological parameters in source-to-sink systems: A basis for predicting semi-quantitative characteristics in subsurface systems: Basin Research, v. 21, p. 361–387, https://doi.org/10.1111/j.1365-2117.2009.00397.x.

Speranza, F., Maniscalco, R., Mattei, M., Di Stefano, A., Butler, R.W.H., and Funiciello, R., 1999, Timing and magnitude of rotations in the frontal thrust system of southwestern Sicily: Tectonics, v. 18, p. 1178–1197, https://doi.org/10.1029/1999TC900029.

Speranza, F., Maniscalco, R., and Grasso, M., 2003, Pattern of orogenic rotations in central-eastern Sicily: Implications for the timing of spreading in the Tyrrhenian Sea: Journal of the Geological Society [London], v. 160, p. 183–195, https://doi.org/10.1144/0016-764902-043.

Speranza, F., Hernandez-Moreno, C., Avellone, G., Gasparo Morticelli, M., Agate, M., Sulli, A., and Di Stefano, E., 2018, Understanding paleomagnetic rotations in Sicily: Thrust vs. strike-slip tectonics: Tectonics, v. 37, no. 4, p. 1138–1158, https://doi.org/10.1002/2017TC004815.

Sweeney, J.J., and Burnham, A.K., 1990, Evaluation of a simple model of vitrinite reflectance based on chemical kinetics: American Association of Petroleum Geologists Bulletin, v. 74, p. 1559–1570.

Tanner, D.C., Behrmann, J.H., and Dresmann, H., 2003, Three-dimensional retro-deformation of the Lechtal Nappe, northern Calcareous Alps: Journal of Structural Geology, v. 25, no. 5, p. 737–748, https://doi.org/10.1016/S0191-8141(02)00057-3.

Tavani, S., Storti, F., Lacombe, O., Corradetti, A., Muñoz, J.A., and Mazzoli, S., 2015, A review of deformation pattern templates in foreland basin systems and fold-and-thrust belts: Implications for the state of stress in the frontal regions of thrust wedges: Earth-Science Reviews, v. 141, p. 82–104, https://doi.org/10.1016/j.earscirev.2014.11.013.

Tavarnelli, E., and Peacock, D., 1999, From extension to contraction in synorogenic foredeep basins: The Contessa section, Umbria-Marche Apennines, Italy: Terra Nova, v. 11, p. 55–60, https://doi.org/10.1046/j.1365-3121.1999.00225.x.

Thomson, S.N., 1994, Fission track analysis of the crystalline basement rocks of the Calabrian arc, southern Italy: Evidence of Oligo-Miocene late orogenic extension and erosion: Tectonophysics, v. 238, p. 331–352, https://doi.org/10.1016/0040-1951(94)90063-9.

Vignaroli, G., Rossetti, F., Theye, T., and Faccenna, C., 2008, Styles and regimes of orogenic thickening in the Peloritani Mountains (Sicily, Italy): New constraints on the tectono-metamorphic evolution of the Apennine belt: Geological Magazine, v. 145, p. 552–569, https://doi.org/10.1017/S0016756807004293.

Vitale, S., Ciarcia, S., Mazzoli, S., and Zaghloul, M.N., 2011, Tectonic evolution of the 'Liguride' accretionary wedge in the Cilento area, southern Italy: A record of early Apennine geodynamics: Journal of Geodynamics, v. 51, p. 25–36, https://doi.org/10.1016/j.jog.2010.06.002.

Whitchurch, A.L., Cartera Sinclair, H.D., Duller, R.A., Whittaker, A.C., and Allen, P.A., 2011, Sediment routing system evolution within a diachronously uplifting orogen: Insights from detrital zircon thermochronological analyses from the south-central Pyrenees: American Journal of Science, v. 311, p. 442–482, https://doi.org/10.2475/05.2011.03.

Zarcone, G., Petti, F.M., Cillari, A., Di Stefano, P., Guzzetta, D., and Nicosia, U., 2010, A possible bridge between Adria and Africa: New palaeobiogeographic and stratigraphic constraints on the Mesozoic palaeogeography of the Central Mediterranean area: Earth-Science Reviews, v. 103, p. 154–162, https://doi.org/10.1016/j.earscirev.2010.09.005.

Zattin, M., Andreucci, B., Jankowski, L., Mazzoli, S., and Szaniawski, R., 2011, Neogene exhumation in the Outer Western Carpathians: Terra Nova, v. 23, p. 283–291, https://doi.org/10.1111/j.1365-3121.2011.01011.x.

Science Editor: Bradley S. Singer
Associate Editor: Stefano Mazzoli

Manuscript Received 9 July 2018
Revised Manuscript Received 26 November 2018
Manuscript Accepted 30 January 2019

Printed in the USA